UNIVERSITY OF BUCHAREST
INSTITUTE OF ATOMIC PHYSICS

LASER – MATTER INTERACTIONS: PROCESSING OF POLYMERIC THIN FILMS FOR BIOMEDICAL APPLICATIONS

Thesis extended abstract defended by

Rodica CRISTESCU

In order to obtain the degree of

Doctor of Philosophy of the University of Bucharest

Discipline : **Physics**

Scientific Supervisor : **Prof. Dr. Ion N. MIHAILESCU**

BUCHAREST
2005

To my child, Cristian,

who will understand my sacrifices of all these years…

UNIVERSITATEA BUCURESTI
Nr. 287 din 15.06.2004

CATRE

……..

Va aducem la cunostinta ca in ziua de 7 ianuarie 2005, ora 9.30, in Amfiteatrul A1 al Facultatii de Fizica va avea loc sustinerea publica a tezei de doctorat, pentru obtinerea titlilui de Doctor in Fizica, cu titlul :

INTERACTIUNEA RADIATIEI LASER CU SUBSTANTA:

PROCESAREA LASER A FILMELOR SUBTIRI DE POLIMER PENTRU APLICATII BIOMEDICALE

RODICA CRISTESCU

Comisia de doctorat este formata din :

Presedintele comisiei :
Profesor Dr. Stefan Antohe, Decan al Facultatii de Fizica, Universitatea Bucuresti

Conducator stiintific:
Profesor Dr. Ion N. Mihailescu, Institutul National de Cercetare-Dezvoltare pentru Fizica Laserilor, Plasmei si Radiatiei, Sectia Laseri, Laborator « Interactiuni Laser-Suprafata-Plasma »

Referenti :
Profesor Dr. Iancu Iova, Facultatea de Fizica, Universitatea Bucuresti
Profesor Dr. Miroslav Jelinek, Institute of Biomedical Engineering of the Czech Technical University, and Institute of Physics, Czech Academy of Sciences, Prague, Czech Republic
Profesor Dr. Douglas B. Chrisey, United States Naval Research Laboratory, Washington, D.C., USA.

In conformitate cu instructiunile Ministerului Educatiei si Cercetarii privind acordarea titlurilor stiintifice, va trimitem alaturat rezumatul Tezei de Doctorat, cu rugamintea de a ne comunica in scris (in doua exemplare) observatiile dumneavoastra, pe adresa Institutului de Fizica Atomica (biroul Doctorate), pana la data de 6 ianuarie 2005.

CONTENTS

If our small minds, for some convenience, divide this…Universe into parts - physics, biology, chemistry, geology, astronomy, and so on – remember that nature does not know it!

Richard P. Feynman, 1963

I. INTRODUCTION

Nano is one billionth of a meter. When a material reaches nano, its characters are changed to new ones. These materials which are neither atomic, molecular nor macro are called nanomaterials.

Nano- and biotechnology have matured as sciences in the last forty-five years from the germ of an idea by Richard P. Feynman (who would win the 1965 Nobel Prize in Physics) to a rapidly growing international research field. At the very end of the decade, on December 29, 1959, at the California Institute of Technology in Pasadena, Richard Feynman gave a talk to the American Physical Society, "There's Plenty of Room at the Bottom" [1]. He said that "there are tremendous innovation space between micro and macro." He predicted that "when we take charge of minute matters, our understanding for material physics will be greatly enriched". The talk also outlined the possibility of using DNA for computers and the potential ability to "use living organisms to build tiny machinery, not just for information storage but for manipulation and manufacturing". Feynman envisioned billions of what he called 'tiny factories' making copies of themselves as well as manufacturing all manner of things. Since 1959, many scientists and technologists have been inspired by Feynman's ideas and have attempted to implement them in an emerging capability for molecular manufacturing, nano- and biotechnology. The results show impressive progress to-date but the most optimistic applications are still far to achieve.

Although only recently accepted as "mainstream" by the R&D community, nano- and biotechnology research is now populated by eminent researchers in such fields as physics, chemistry, molecular biology, and computer science. These fields have become interdisciplinary and continuously expansive: impressive large conferences are organized; scientific books are edited by leading publishers: Kluwer, Elsevier, John Wiley & Sons, Academic Press; articles appear with increasing frequency in the main flux of publications.

One of the principal challenges in solid-state physics, surface chemistry, and materials science, is the discovery and application of novel materials and their incorporation in devices for use in areas as diverse as biophysics, optoelectronics, nano- and biotechnology.

An important class of materials of interest for nano- and biotechnology consists of *biomaterials*. Biomaterials have been defined as substances other than foods or drugs contained in therapeutic or diagnostic systems and, in some cases, have been described as materials composed of biologically derived components irrespective of their application. Biomaterials have played an enormous role in the success of medical devices and drug delivery systems. They include *natural tissues* (collagen, bones, mother of pearl, coral), *metals and alloys* (Fe-based, Ti-based, Au-based, Ag-based, Pd-based, dental amalgams) and *ceramics* (marble, oxides, phosphates, bioglasses). Also *composites* (different synthetic biomaterials: ormosils - organically modified silicates, and ormocers -organically modified ceramics, synthetic biomaterials combined with natural tissues: collagen with polylactic–co-glycolic acid (PLGA)) are of interest nowadays. In addition, *active biomaterials* (biological glues, synthetic biomaterials impregnated with antibiotics, antimitotics and growth factors) are evidenced [2].

A special class of biomaterials consists of *polymers*: current polymers: polymethil-methacrylate (PMMA), hydroxyl-ethyl-methacrylate (HEMA), polyethylene (PE), unresorbable polymers: poly-tetra-fluoro-ethylene (PTFE), polyurethane (PU), silicones, and resorbable polymers: hyaluronic acid, polylactic acid (PLA), polyglycolic acid (PGA), PLGA, and proteoglycans. *Biopolymers* (dextrans, chitosan, *pullulan*, polysaccharides and peptides) and proteins (silk, elastin, collagen, cheratin, *fibrinogen*, enzymes, DNA and RNA) have been recently addressed by research groups. Lately the research is focused on processing biomimetic proteins such as spider dragline silk- *Latrodectus Hesperus*, (that ounce for ounce, is five times as strong as steel and five times as impact-resistant as bulletproof Kevlar) and *Mytilus edulis* adhesive proteins –the underwater superglue made by mussels [3].

As noticed, *polymers* play an important role in biomedical applications. Novel polymeric materials including biodegradable polymers, polymeric hydrogels, functionalized biocompatible polymers and undegradable biocompatible polymers are under evaluation. On the other hand, living matter is able to synthesize an overwhelming variety of polymers. This special class of polymers includes *biopolymers* and *proteins*. They mostly are biodegradable. This property demonstrates advantages when applied as uniform and adherent thin films and structures in controlled drug delivery and tissue engineering.

New trends in biomaterial development are based on different techniques of functionalization: mechanical, physical, chemical and biological. One area that researchers have particularly been focused on consists of physical methods to deposit thin films and structures: treatment with hot plasma, chemical vapor deposition, sol-gel coating, hydrothermal treatment, and laser technologies.

Polymers, biopolymers and proteins do not naturally occur as thin films. On the other hand, they may be processed into thin films. These biomaterials thin films should closely resemble the bulk material, with minimal fragmentation, rearrangement, and degradation. Many different approaches exist to material transfer. Each technique has its own merits and shortcomings. Thin polymeric and organic films can be deposited by a wide variety of techniques that range in their complexity and applicability. The selection of deposition technique to use depends upon the physicochemical properties of the material, the requirements for film quality, the substrate that is being coated, and the costs. The simplest methods involve the application of a liquid solution of a polymer in a volatile solvent, including aerosol, dip coating, and spin

coating [4]. There are some techniques that are applicable to bulk polymer materials, including vacuum evaporation [5] and pulsed laser deposition or ablation [6-8]. Finally, there are techniques that involve in situ polymerization of monomer using plasma [9], electrochemical [10], catalytic, or photoactivated processes [11, 12] to convert the starting material or monomer to a polymer on a substrate surface. For organic thin films, Langmuir-Blodgett dip coating using self-assembled monolayers is the most common method to functionalize surfaces with single biomolecular layers [13, 14]. However, each of the above-mentioned techniques only work certain types of compounds and are not generic enough to be used with a wide variety of polymeric and organic materials to be deposited as thin, uniform and adherent coatings over an extended substrate surface area, or in localized areas with accurate and precise thickness control, while maintaining their chemical integrity and desired physicochemical properties. Furthermore, most of these techniques are not appropriate for the fabrication of multilayers, since they rely in the application of a solvent solution containing the material of interest which can dissolve any prior deposited layers. Next generation applications call for tighter tolerances on the structural, morphological, and chemical composition of the required thin films. For electronic, optical and biosensors device applications, the materials of choice cover a wide range from polymeric materials for the fabrication and passivation of electronic coatings, to organic dye molecules for non-linear and optical limiting applications, and biocompatible and protein coatings for micro-array biosensor applications. Obviously, the ability to deposit various classes of functional polymeric and organic materials using a single technique provides a significant advantage for their development and implementation.

The aforementioned drawbacks potentially could be addressed by the laser processing because of its advantages, e.g., monolayer thickness control, the enhanced film-substrate adhesion, compatibility with non-contact masking techniques and minimum possible degradation.

Pulsed Laser Deposition (PLD) is a well-known method of laser processing of stoichiometric, adherent, and uniform thin films. Unfortunately, conventional PLD is unacceptable, with a few exceptions (i.e., polytetraflouroethylene) for deposition of complex organic molecules especially polymers and biomaterials (biopolymers and proteins). This is a consequence of the fact that ultraviolet laser-polymer interaction usually result in photochemical damage of the transferred material.

In the search for a universal approach to producing high-quality thin films, a new vapor deposition technique, *Matrix Assisted Pulsed-Laser Evaporation* (MAPLE), has emerged. The patented process [15], developed at the Naval Research Laboratory in Washington, DC, can generate high quality polymeric, organic, and biomaterial films on many types of substrates. The technique has been used to deposit a wide range of organic and inorganic polymers, biopolymers, and low to intermediate molecular weight organics as thin, high quality, uniform, and adherent coatings. These films are grown - with areas of a few square micrometers and in thicknesses ranging from 5 nm to several micrometers - over extended areas without degrading the physicochemical properties of the deposited materials. To date, the technique has been used for processing thin films of polymers and biomaterials ranging from macromolecules as large as 600 kDa, such as hydrogels, to small molecular species less than 200 Da, such as sugars. Furthermore, its ability to deposit films of complex polymeric and organic materials has been demonstrated for a wide variety of chemoselective polymers and plant and animal proteins, without damage to their structure or effect on their chemical or biological activity.

In our country optics, spectroscopy, lasers plasma research and technology have a long tradition extending over half century [16-18]. Laser ablation studies have been started about 15 years ago. They naturally developed as a consequence of 20 years of investigations of plasma generation and diagnostic. During years, there were obtained films and complex structures, starting from ceramic or metallic targets. These investigations have been performed mainly in the Lasers Department from National Institute for Lasers, Plasma and Radiation Physics, and have been facilitated by numerous internal and international collaborations [2, 19- 34].

This thesis performed within the aforementioned general framework was particularly possible during last years by initiation and development of a fruitful scientific and technological collaboration with Professor Douglas B. Chrisey from United States Naval Research Laboratory (NRL). He is the well-recognized inventor of MAPLE and MAPLE Direct Write techniques. Also, I worked with the Professor Chrisey's collaborators teams led by Professor Roger J. Narayan and Professor Boris Mizaikoff from Georgia Institute of Technology. These collaborations have been materializated by the most recent results in the thesis. During this research I have contacted and initiated scientific collaborations with Professor Phillip B. Messersmith from Biomedical Engineering Department from Northwestern University, Professor Jonathan Wilker from Department of Chemistry, Purdue University, and Professor Herbert Waite from Cell and Developmental Biology Department, University of California.

The present PhD thesis is novel by extending PLD by implementation and development of MAPLE processing of functionalized polymeric thin films and structures for biomedical applications. They are polymers (PMMA), biopolymers (pullulan), and proteins (collagen and *Mytilus edulis* adhesive protein analogs). I emphasize that materials used for elaborating this thesis were selected on the basis of their remarkable biocompatibility and biodegradability which strongly recommend them for top biomedical applications.

This thesis is structured on chapters and sections.

Next chapter presents materials investigated in this thesis for obtaining polymeric thin films and structures. In Section II.1 biomaterials will be introduced pointing out recent research trends on interdisciplinarity between material science, biophysics and biochemistry for biomedical applications. Section II.2 includes definitions, properties and

classifications of polymers, biopolymers and proteins. Section II.3 is dedicated to concepts of controlled drug delivery and tissue engineering. Section II.4 describes in detail studied biomaterials and their potential applications.

The Chapter III is devoted to basic principles and phenomena of experimental methods. Section III.1 presents laser induced absorption and desorption. In Section III.2 PLD method is described stressing on advantages and main characteristics. Section III.3 introduces MAPLE technique and its progress obtained up to now in the field. Section III.4 presents the experimental setup. Section III.5 describes in detail laser parametric values, and experiments performed for growing thin films and structures of studied biomaterials. Section III.6 shortly presents the complementary investigation methods and devices used for characterization of thin films and structures from the point of view of composition and surface morphology.

Chapter IV contains the original results and their interpretation in order to evaluate the influence of laser parameters related to synthesis and characterization of thin films and structures of polymers, biopolymers and proteins. Section IV.1 is devoted to the results in case of PLD of PMMA and pullulan. Section IV.2 points out the results in case of MAPLE of pullulan, collagen and *Mytilus edulis* adhesive protein analogs.

The final chapter contains the conclusions of the thesis.

All references are collected in the end of the thesis.

II. MATERIALS

II.1. Biomaterials

Biomaterials are materials destined to be put in contact with living systems and/or with biological fluids in order to evaluate, treat, modify forms or replace any tissue, organ or function of the body. The interaction between materials and living systems is dynamic and complex. It involves the response of the living system to the materials (e.g., *biocompatibility* and *bioactivity*) and the response of the materials to the living system (e.g., *biodegradation*).

In addition, a biomaterial must possess certain essential qualities. Once implanted in the body, it must be as *resistant* as possible: mechanical resistance and corrosion resistance to chemical dissolution and electrochemical corrosion. The choice of biocompatibility assays is based on the *knowledge of toxicological factors* which control it: chemical, electrical, and geometric factors, surface properties of the materials and mechanical interactions tissue/material. On the other hand, the material or its degradation products must be neither responsible for inflammatory reactions, susceptible to generate allergic or immun reactions, toxic, mutagenic nor carcinogenic. Another argument for biocompatibility is also added to the requirement output of a biomaterial, i.e. *its complete sterility*. This is in particular applied to biomaterials of human or animal origine free of any contamination: proteins generating immun or other unwanted reactions, virus or virus fragments inducing highly severe consequences.

The requirements for biological environment are a critical factor in limiting the myriad of possible metal, polymer, and ceramic compositions to a relatively small number that to date have been proven useful in medical devices. The new generation of biomaterials must be recognized and accepted by human cells, must aid in the natural process of bodily repair, and, ultimately, must promote the regeneration of tissues.

Biomaterials have played an enormous role in the success of medical devices and drug delivery systems [35]. The new challenges and directions in biomaterials research include:

i. promoting synthetic replacements for biological tissues using naturally occurring building blocks including extracellular matrix (ECM) components are being studied for applications such as direct tissue replacement and tissue engineering,

ii. synthesizing materials using manmade building blocks for specific medical and biological applications, and

iii. developing materials for new in vitro applications such as diagnostics and array technologies.

II.2. Definitions, properties and classifications

Polymers are natural or synthetic substances formed by the linkage (polymerization) of two or more simple, unsaturated molecules (called monomers), to form a single heavier molecule having the same elements in the same proportions as the original monomers. Synthetic polymers are formed by addition or condensation polymerization of monomers. An addition polymerization is the polymerization where the entire monomer molecule becomes part of the polymer. A condensation polymerization is the polymerization where part of the monomer molecule is kicked out when the monomer becomes part of the polymer.

*Biopolymer*s are natural macromolecular polymeric substances formed by association of small molecules by biologic systems or living bodies. In case of biopolymers, the repetitive structural units are sugars, amino- and nucleic acids. Living matter is able to synthesize an overwhelming variety of polymers, which can be divided into eight major classes according to their chemical structure: (1) nucleic acids: ribonucleic and deoxyribonucleic acids, (2) polyamides: *proteins* and poly(amino acids), (3) *polysaccharides*: cellulose, *pullulan,* starch and xanthan, (4) organic polyoxoesters: poly(hydroxyalkanoic) and poly(malic) acids, and cutin, (5) polythioesters, reported only recently, (6) inorganic polyesters with polyphosphate, (7) polyisoprenoids: natural rubber or Gutta Percha, and (8) polyphenols: lignin or humic acids [36]. Biopolymers and their derivatives are diverse, abundant, and important for life; they exhibit fascinating properties and are of increasing significance for various applications: drug delivery, tissue engineering, cell modification, synthetic organs and other intelligent functions. For example, *polysaccharides* are used as aditives, and desintegration or suspention agents in drug formula.

An important class of biopolymers consists of *proteins*. *Proteins* are a diverse class of biological chain molecules (natural polymers) that act as nano-machines, performing the basic functions of life at the molecular level in all organisms. By analogy to macroscopic machines, there is a strong relation between 3D-structure and function. The analysis of protein structure is the key to a thorough understanding of protein function and dysfunction. New ways to speed up structure analysis by a direct coupling of experiments and bioinformatics are explored. Their structure is schematically presented in Fig. II.1:

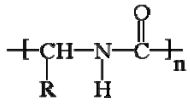

Fig. II.1. Protein chemical structure.

A protein is a naturally occurring polyamide. That is a polymer containing an *amide group* in the backbone chain. Fig. II.2 gives an amide group, and next to it, a polyamide:

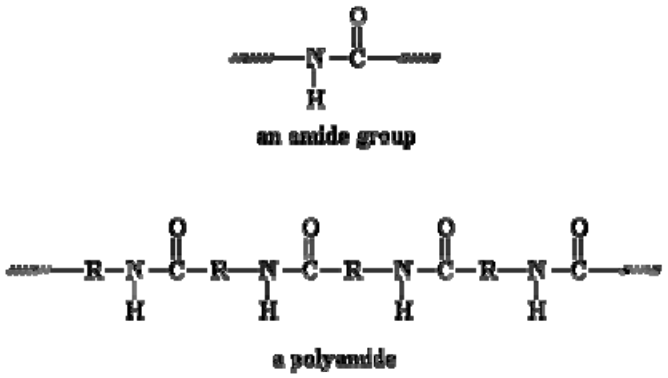

Fig. II.2. Chemical structures of an amide group and a polyamide.

In proteins, the *R* group placed between amide groups, is a single carbon atom, with two pendant groups attached (Fig. II.3). One pendant is always a hydrogen atom, and the other could be any chemical radical *R'*:

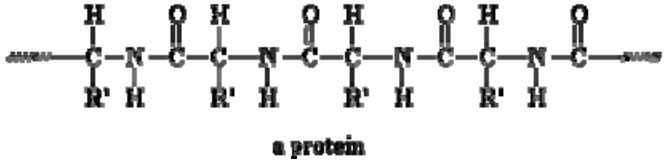

Fig. II.3. Protein chemical structure.

In the body, these proteins are made from monomers called *amino acids*, like in Fig. II.4:

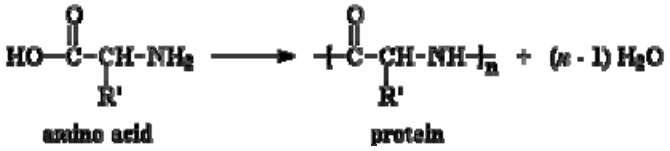

Fig. II.4. Synthesis of protein from aminoacid.

Each amino acid has a different *R'* group. Also, each protein has a specific sequence of the different amino acids. For each protein, there is a different sequence of *R'* groups hanging off of the backbone chain. This sequence determines the properties of the protein. There are twenty different amino acids (Table II.1)**.**

Table II.1 The 20 amino acids represented in the genetic code

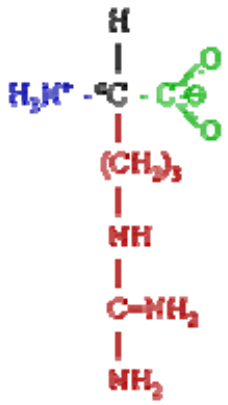 Arginine (Arg / R)	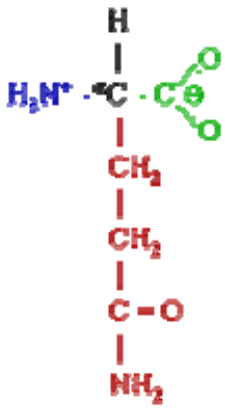 Glutamine (Gln / Q)	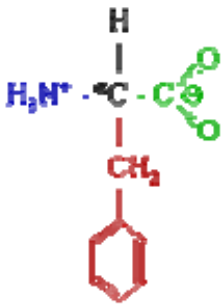 Phenylalanine (Phe / F)	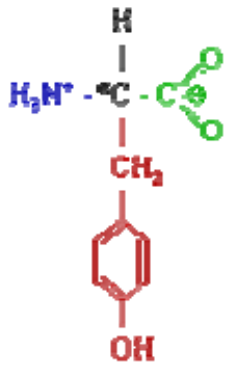 Tyrosine (Tyr / Y)	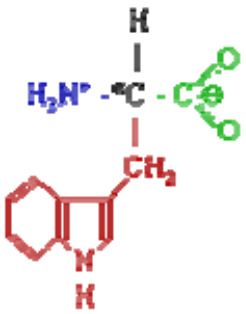 Tryptophan (Trp, W)
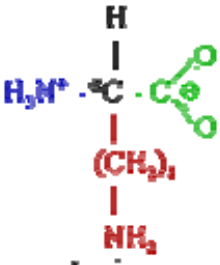 Lysine (Lys / L)	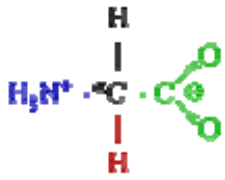 Glycine (Gly / G)	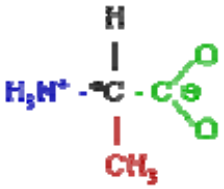 Alanine (Ala / A)	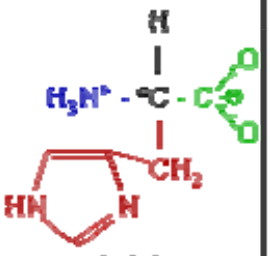 Histidine (His / H)	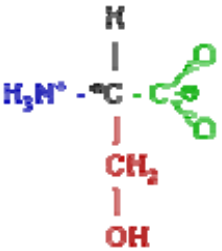 Serine (Ser / S)
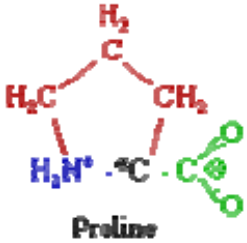 Proline (Pro / P)	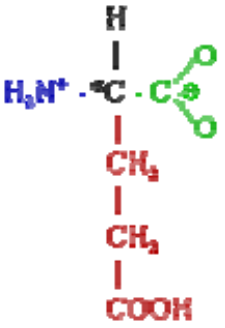 Glutamic Acid (Glu / E)	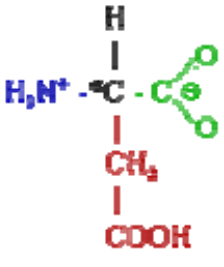 Aspartic Acid (Asp / D)	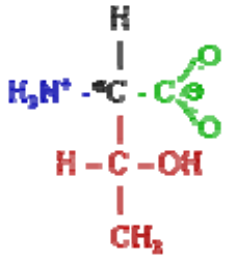 Threonine (Thr / T)	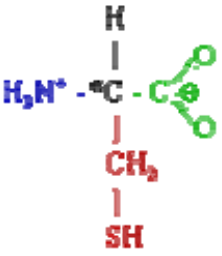 Cysteine (Cys / C)
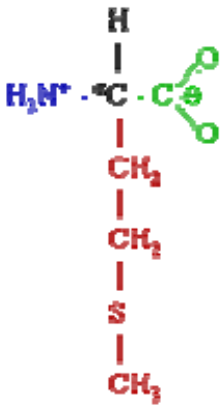 Methionine (Met / M)	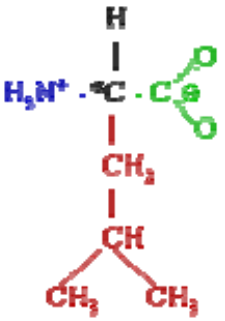 Leucine (Leu / L)	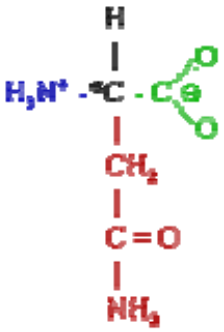 Asparagine (Asn / N)	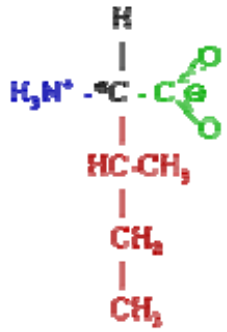 Isoleucine (Ile / I)	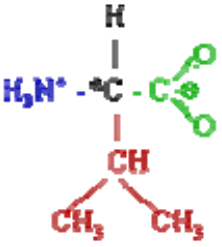 Valine (Val / V)

II.3. Drug delivery and tissue engineering

Drugs are any chemical compounds that may be used on or administered to humans as an aid in the diagnosis, treatment, cure, mitigation, or prevention of disease or other abnormal conditions.

Oral solid dosage formulations are a convenient method of drug delivery and account for a large proportion of pharmaceutical products. Drug substances are not routinely administered in the pure state, and functional components is a heterogeneous mixture of many components, with individual particles of the order of micrometers in size. Additionally, solid dosage design can include strategies to precisely control the rate of drug delivery (for example, sustained release), typically using one or more polymer coatings which must reach a specific body site and possess an appropriate release profile [37-38].

Ideal performances of drug delivery systems are:

i. to have a minimal effect dose;
ii. to be easy to administer;
iii. to be highly targeted;
iv. to posses a correct time response;
v. to have minimal side effects (i.e., toxicity).

Another type of material being developed for drug delivery is the so-called *intelligent biomaterials*. Such materials would combine molecular recognition with drug release. This strategy represents the future of drug delivery. A new generation of drug delivery systems, consists of *polymers* able to recognize certain compounds by using the technique of molecular imprinting, which is more often associated with chromatography. The molecule that the polymer/biopolymer/protein will sense is used as a template around which the monomers are allowed to polymerize. The template molecule is then extracted from the polymer. These special materials are used in cancer treatment and tumoral extractions.

An advantage of use of polymers, including here biopolymers and proteins, is that the linkage can be designed to control where and when the drug is released. For instance, bioadhesive polymers – *Mytilus edulis* adhesive proteins analogs - can improve the absorption of drugs. There are applications for bioadhesive polymers in almost any region with epithelial cells. The adhesive molecules bring the delivery system closer to the mucosa.

Another application in which drug delivery and materials (polymer, biopolymer, protein) development play a key role is *tissue engineering*. At a National Science Foundation Workshop held in 1988, the term "*tissue engineering*" was officially defined as, "the application of principles and methods of engineering and life sciences toward fundamental understanding of structure-function relationships in normal and pathological mammalian tissue and the development of biological substitutes to restore, maintain or improve tissue function." Ideally, this concept of treatment could be applied to cartilage restoration for patients suffering from cartilage damage. Although this therapy is far from routine, it presents some advantages compared with other currently used techniques. First, the tissue product is made entirely of biological materials. Additionally, the manipulation of the artificial environment enables the growth of 3-D, fully functional cartilage substitutes that are immuno-compatible with the host. Finally, the scale-up made possible through the culture of such bioartificial substitutes solves the problem of the critical donor shortage limiting the application of the transplantation technique. Under ideal conditions, tissue engineering would produce and maintain sterile cartilage tissues with defined shape and size that can be inserted in a patient's body through traditional surgery. The success of the tissue-engineering technique depends mostly on the production of constructs able to mimick compositional and mechanical properties of the native cartilage and the achievement of the functional integration between the tissue-engineered constructs and the surrounding articular cartilage following implantation. By combining polymers with mammalian cells, it is now possible to make skin for patients who have burns or skin ulcers. Various other polymer/cell combinations are in clinical trials, including corneas, cartilage, bone and liver [39].

II.4. Investigated materials

II.4.1. Polymethyl methacrylate (Polymethyl Methacrylic Acid, PMMA)

Polymethyl methacrylate known as PMMA is a transparent biocompatible polymer, used as a shatterproof replacement for glass. Its chemical structure is given in Fig. II.5.

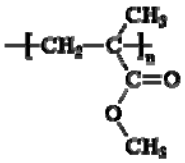

Fig. II.5. Chemical structure of PMMA

PMMA is an addition polymer, made by free radical vinyl polymerization from the monomer methyl methacrylate (Fig. II.6).

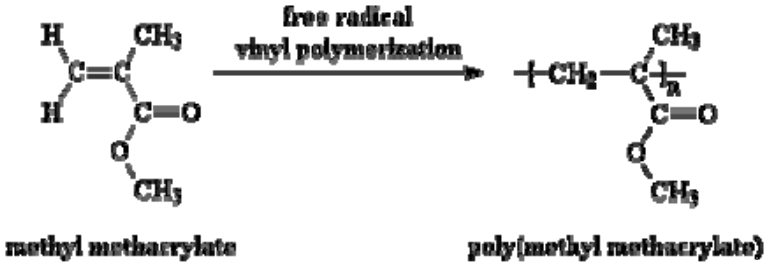

Fig. II.6. Polymerization reaction of PMMA.

Some selected thermodynamic properties of PMMA are summarized in Table II.2 [40].

Table II.2. Selected thermodynamic properties of PMMA.

Property	Symbol (Units)	Value
Density	ρ (g/cm^3)	1,19
Specific heat (solid)	C_P (J/g.K)	1,40
Thermal conductivity	k (W/m.K)	0,21
Penetration depth (for irradiation at 248 nm)	1 / α(nm)	200
Thermal diffusion length	$l(t) = \sqrt{\frac{kt}{\rho c}}$ (nm)	42

The thin films of PMMA are used for many applications (Table II.3) such as: electron-beam litography, laser nanolitography, direct writing, coatings, X-ray resist, photoresist, optical fibers, optical lens, chemical sensors, holographic network, holographic memories, data storage and display applications**.**

Table II.3. Requirement and potential use of thin films of PMMA.

No	PMMA thin film requirements	Potential use
1	High transmisivity.	The light integration applications (lighter projector), optic and photografic devices.
2	Good resistance in time and under atmospheric agents, transmitance lower than 1% after 5 years.	The protection from atmospheric agents.
3	Umidity absorbtion lower than 1,5%, good resistance to exposure on alcalies, acids, salts and sea water.	Coatings.
4	Precise thickness and overall uniformity.	Chemical sensors.
5	Electret with good charge storage.	Data storage and display applications.
6	Remarkable physical, chemical and mechanical stability, neither degradabil nor bioactive.	The field of orthopedics as a bone cement for implant fixation, repair of certain fractures and bone defects (i.e. osteoporotic vertebral bodies).

II.4.2. Pullulan

Pullulan (Fig. II.7) is a natural water-soluble polysaccharide. Pullulan is obtained by fed-batch fermentation of glucose by the fungus *Aureobasidicum pullulans. A. pullulans* is ubiquitously found in nature; it is nontoxic and nonpathogenic. The reports of adverse events associated with *A. pullulans* as extremely rare, restricted to immuno-deficiency and other high risk individuals, or due to misidentification of the organism. Molecular weights for pullulan range from 8,000 to 2,000,000 daltons depending on the growth conditions of the organism. It is often described as an amorphous biopolymer which contains glucopyranozic units linked α (1→4) and α (1→6).

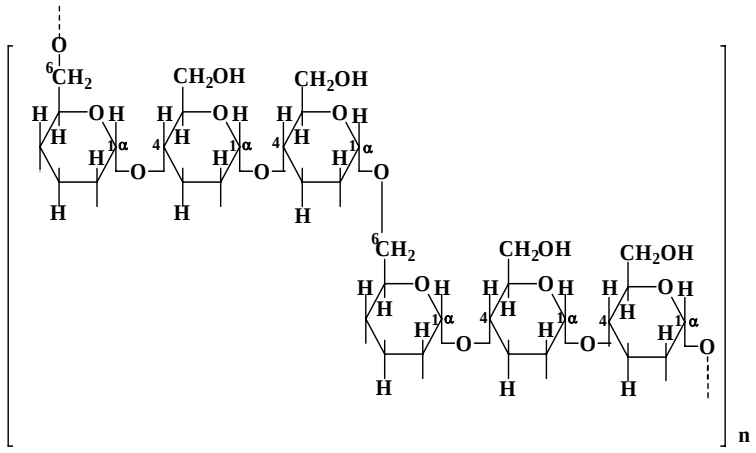

Fig. II.7. Chemical structure of pullulan

This configuration confers to pullulan specific physical remarcable characteristics. Pullulan has adhesive properties and readily forms a film, which is thermally stable, anti-static, elastic and impermeable for oxygen. It decomposes at 250 to 280 ^{o}C, is non-hygroscopic and non-reducing. In addition, pullulan has a high affinity for the liver when conjugated with interferon [41].

Pullulan was first reported in 1938. The commercial manufacturing has started in 1976 by Hayashibara Biochemical Laboratories, Inc., in Japan [42]. Pullulan has numerous applications including foods, pharmaceuticals, and cosmetics, primarily due to its membrane-formation characteristics, adhesion, and edibility. It is also easy to process into films, sheets, and shaped goods, and has been referred to as an "edible plastic" [43]. Nevertheless, the last few years have seen resurgence in interest in pullulan, particularly for higher-value health and pharmaceutical applications.

In our experiments we used pullulan made in this country (P-20 type) following an patented original method by the National Institute for Chemical-Pharmaceutical R&D, Bucharest, Romania [44]. Molecular weight of pullulan used in our experiments is 200,000 Da.

II.4.3. Collagen

The collagens form a family of proteins that constitute the major structural components of the extracellular matrix (ECM), representing approximately one-third of proteins in the human body.

ECM is a structural and functional entity composed of an assembly of many macromolecules that fill the spaces between cells. It is composed of a variety of versatile proteins and polysaccharides that are secreted locally and assembled into an organized network in close association with the cells that produce them. ECM plays a critical role not only in determining the three-dimensional arrangement of cells in tissues, but also in controlling the growth, movement, differentiation, and cooperation of each cell in those tissues.

The proteins that comprise ECM are classified into two types: the structural glycoproteins such as *collagen* and elastin, and the proteoglycans. Together, these proteins impart tremendous strength and flexibility to tissues while also serving as a selective filter to control the flow of undissolved particulate material between cells. The proteoglycans also attract water, thereby maintaining a hydrated environment around cells.

The principal function of collagens is to provide structural support to tissues. Collagen subunits are secreted from cells and then assembled into larger fibrils and fibers in the extracellular space.

Collagen is a polypeptide secreted by fibroblasts. The collagens make up the main protein component in all connective tissues, including skin, cartilage, bone, tendon, ligament and blood vessels. Collagens come in a variety of

shapes organized into different structures. The types of collagens are different by morphology, aminoacid composition and physical properties.

Collagen occurs in many places throughout the body, and is present in different forms known as types:

i. type I collagen, the most abundant kind of collagen of human body (representing 90 % of body collagen). It is present in tendons, skin, bone, tendons and most other connective tissues, scar tissue, the end product when tissue heals by repair;

ii. type II collagen is found in articular cartilage;

iii. type III collagen is identified in granulation tissues. It is quickly produced by young fibroblasts before the tougher type I collagen is synthesized;

iv. type IV collagen is present in basement membrane.

Collagens are a family of over 20 different extracellular matrix proteins and are the most abundant proteins in the animal kingdom [45].

All proteins of the collagen family have a common property: they are bundled together as thin (approximately 1.5 nm diameter), triple helical, coiled coils composed of three collagen protein subunits, held together by both noncovalent and covalent bonds.

Collagens contain a characteristic repeating sequence of amino acids consisting of Gly-X-Y, where Gly is Glycine X and Y can be any amino acid but are usually proline and hydroxyproline, respectively (Table II.1). This sequence enables tight packing of the three subunits and facilitates coiled-coil formation. Three polypeptide subunits are wrapped together in parallel to form a 300 nm-long coiled coil.

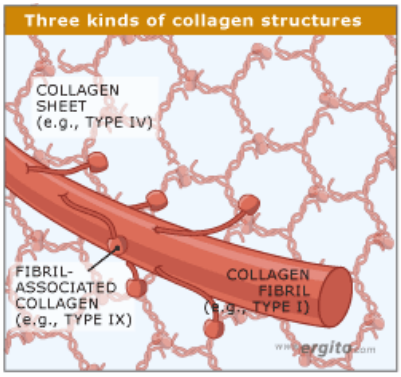

Fig. II.8. Three kinds of collagen structures.

The coiled coils form three kinds of collagen structures—fibrillar, sheet-like, and fibril-associated, as illustrated in Fig. II.8:

i. fibrilar collagen: have coiled coils organized into fibrils, or "ropes," that provide great strength along a single axis. When these fibrils are clustered into parallel bundles, such as in tendons, they impart tremendous strength capable of resisting the strain imposed by muscles on bones;

ii. sheet-like collagen have coiled coils organized into networks that, while less able to resist muscular force, are better able to withstand stretching in multiple directions; these networks are found in skin;

iii. fibril-associated collagen have coiled coils used to bind fibrillar collagens (i) together.

The collagen morphology is given in Fig. II.9 a-b.

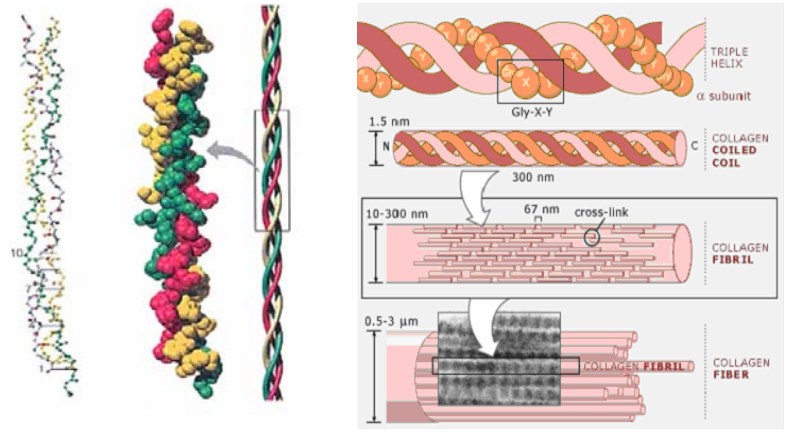

a. *b.*

Fig. II.9. Collagen morphologic structure (a) and details (b).

Collagen has found widespread use in the biomedical field where applications for it in various forms abound. Medical applications in urology, dermatology, orthopaedics, vascular and general surgery utilize collagen in various forms ranging from injectable solutions to sponge-like materials. A broad range of medical applications exist for collagen today as biomaterials for soft tissue repair and also hard tissue repair [39]. These applications include injectable collagens for soft tissue augmentation, dressings for healing wounds and burns, bone repair, and replacement components for the cardiovascular system, such as bioprosthetic heart valves. One important application of collagen in the form of sponges or fleeces is the use as a haemostatic agent in surgery. It exploits the inherent platelet binding property that leads to an initiation of the clotting cascade. Also collagen can be used as a drug delivery system. Collagen is an ideal biomaterial for the development of medical and other commercial products because it is highly biocompatible, is readily available at high purity.

In our experiments we used high quality type I fibrilar collagen [46] made in this country by the Leather and Footwear Research Institute, Bucharest, Romania.

II.4.4. Adhesive proteins extracted from *Mytilus edulis* and their analogs

Mussel adhesive proteins are one of nature's most remarkable and powerful adhesive materials. These substances are secreted by several mussel species, including *Mytilus edulis* (Fig. II.10) and form tenacious bonds between the mussel and the surface it resides on [47].

Fig. II.10. Mytilus edulis *in natural environment*

To attach to a surface, the mussel secretes sticky threads that are soft and rubbery near its body and stiffen to a nylon-like consistency near the surface [48]. The proteins used to make these glues possess both adhesive and elastic qualities. It provides to the glue a combination of strength, stretch and stickiness that is hard to emulate in man-made glues.

The mussel foot creates threads and plaque that keep the shellfish anchored to a surface. The foot inspects the environment for areas with just the right water flow and for slime or debris. Once in a suitable home, the foot goes into a state of paralysis, and a new thread is molded and assembled. When the thread and plaque are fully assembled the foot retracts and moves on to make another thread.

The mechanisms of mussel glue are akin to those of the conventional two-part epoxy glues [49]. Glue glands in the mussel foot produce resin-like proteins in one compartment and hardeners, or curing agents, in another. When released, the agents mix and cure. Recently it was advanced the idea that one of the curing agents could be a metal (copper, zinc or iron). Mussels are filter feeders, pumping water through tiny gills to sift out nutrients in plankton and other material. This filtering mechanism also allows the shellfish to accumulate metals from the seawater. Studies show that mussel concentrations of metals such as iron, zinc and copper can be up to 100,000 times higher than those found in seawater. The new findings suggest that adding iron to two key mussel proteins can, within minutes, create the cross-links needed to transform them into cement [48].

The long-lasting strength of mussel adhesive proteins in seawater is problematic (Fig. II.11); marine biofouling of ships and other underwater structures, remains a major problem. Biofouling on ships reduces their speed and maneuverability, causing increased fuel and maintenance costs. On static structures (e.g. buoys, piers, jetties, offshore oil and gas platforms) biofouling can enhance the corrosion of metal by seawater, reducing the metal susceptibility to environmental fracture, and increasing the risk of mechanical failure.

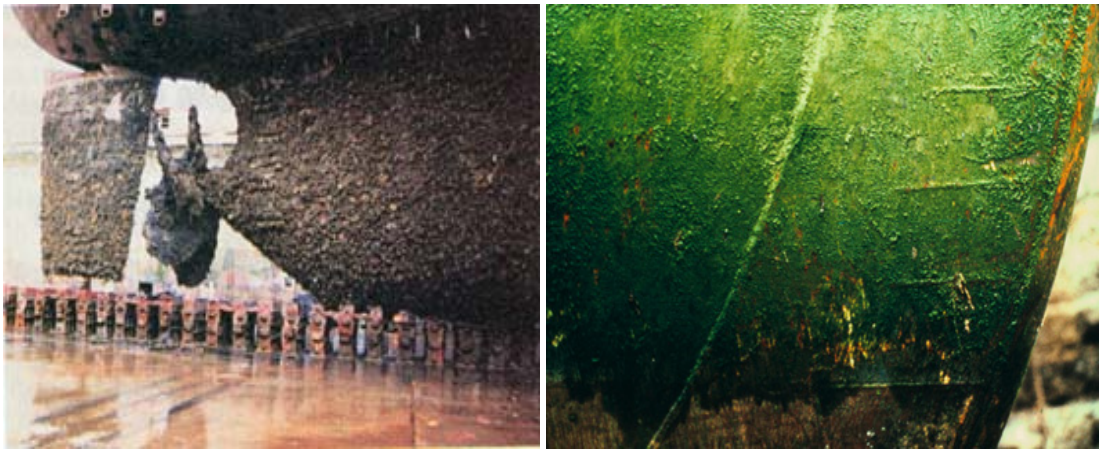

Fig. II.11. Biofouling due to Mytilus edulis *(left) and* Enteromorpha (right*).*

On the other hand, high quality mussel adhesive protein thin films could potentially serve as "mussel glue" with several advantages over conventional adhesives. The mussel adhesive proteins are special in that they function over wide temperature ranges (- 40 – +40) °C, fluctuating salinities, and humidity and in the tides, wave, and currents of marine environments. These materials do not require high temperatures to bond and are not poisonous, unlike conventional petroleum- or tar-based adhesives. The bonding formed by mussel adhesive proteins is permanent and versatile, and requires only one minute to harden. In contrast, the success of synthetic adhesives in wet environments requires carefully cleaned adherence surfaces, which often must also be chemically treated and/or partially dried [50-51].

Mussel adhesive proteins form incredibly strong threads that can bond a variety of substrates with complex and often irregular surface coatings. Here metals, polymers, and living tissues are included [48, 51-52] (Fig. II.12).

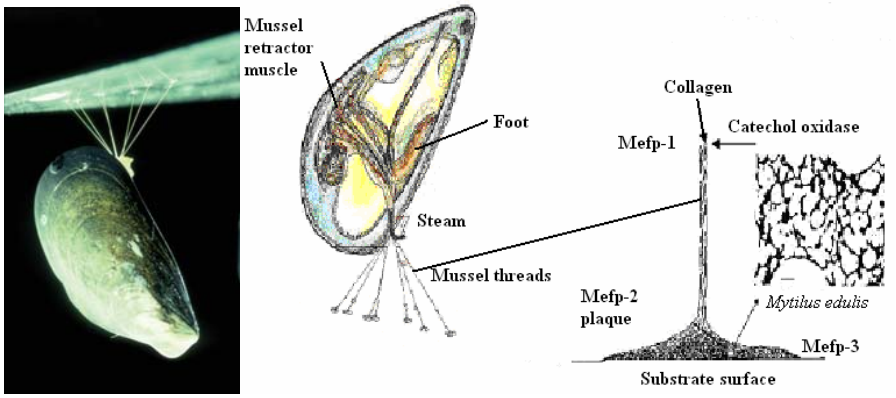

Fig. II.12. Common blue mussel hanging five (or more) after a night adhering to otherwise non-stick Teflon.

This mollusk uses a glue that is not only rapid, strong and efficient, but works in sea water, a churning, wet and saline environment - more or less the same environment as inside our bodies. This remarkable glue is very attractive for a wide variety of medical and technological applications [53-56]. Potential medical applications include use in mending broken bones, eye repair, wound closure, nerve reconstruction, tissue engineering, drug delivery [57], microbial biofilm prevention [58], non-adhesive coatings for metal implants (stents, heart valves or other devices to prevent blood cells and proteins from accumulating).

Technological applications include use as a marine anti-fouling coating to keep barnacles, algae and mussels off ships and oil rigs [51, 59-60], rustproof coatings for cars and bridges and use as an electrically conductive, waterproof adhesive for electronic packaging [61].

Mussel adhesive proteins outperform man-made adhesives in many areas. Unfortunately, these proteins can only be obtained from mussels in very small quantities. Furthermore, extracting this adhesive protein on a large scale directly from the mussel and using it the real thing is time consuming and costly. Moreover, the most important drawback is that commercial harvesting of the glue would soon decimate the mussel population because it takes about 10,000 mussels to extract just one gram of the glue [53].

The main research objective is to develop a biomimetic glue that is environmentally safer, stronger, and less expensive than currently available adhesives. Studies have had a substantial progress in the identification of the genes responsible for the production of mussel adhesive proteins. This work has led both to the development of recombinant

proteins, synthetic polypeptides, and modified polymeric systems that are able to reproduce the properties of natural mussel adhesive proteins [51, 13, 62-63] and identification of at least nine different, unique proteins in the formation of the byssus (the adhesive structure formed by the mussel).

One of the unique features of mussel adhesive proteins is the presence of L-3,4-dihydroxyphenyl-alanine (L-DOPA) (Fig. II.13) - a highly reactive amino acid. This aminoacid has very strong hydrogen bonds and the capability of having metals as ligands.

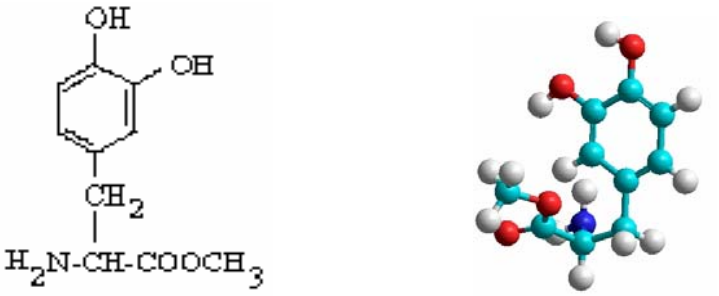

Fig. II.13. Chemical structure and 3-D view of L-3,4-dihydroxyphenyl-alanine (L-DOPA).

L-DOPA (a brain chemical that is the basis for Parkinson's treatments) has been described as a "*polyphenolic*" protein, and is believed to be responsible for both adhesion and crosslinking properties of these materials [51, 53, 62, 64-65].

The mussel adhesive protein contains this sequence of aminoacids: Ala-Lys-Pro-Ser-Tyr-HPro-HPro-Thr-DOPA-Lys (Table II.1, where HPro= Hydroxyproline) [63].

In the thesis we have investigated two analogs of mussel adhesive protein: DOPA-PF68 and DOPA-PF127. They are two L-DOPA modified poly(ethylene oxide)-poly(propylene oxide)-poly(ethylene oxide) block copolymers (DOPA-PEO-PPO-PEO)-MAP analogs [66].

PEO-PPO-PEO triblock copolymers have attracted considerable interest in the biotechnological and pharmaceutical industries for their unique surfactant abilities, low toxicity, and minimal immune response.

Polymer solutions possessing thermogelling and bioadhesive capabilities are potentially useful for medical and dental applications for example as tissue adhesives and as injectable carriers for drug delivery to mucosal surfaces. In an attempt to improve the bioadhesive properties of PEO-PPO-PEO block copolymers, which are known to be poorly bioadhesive, they have been conjugated with biological moieties that are known to possess desirable adhesive properties in nature, such as L-DOPA described above.

The average molecular weights of DOPA-PF68 and DOPA-PF127 are approximately 8,600 and 12,600 Da, respectively. The chemical formula is visible in Fig. II.14.

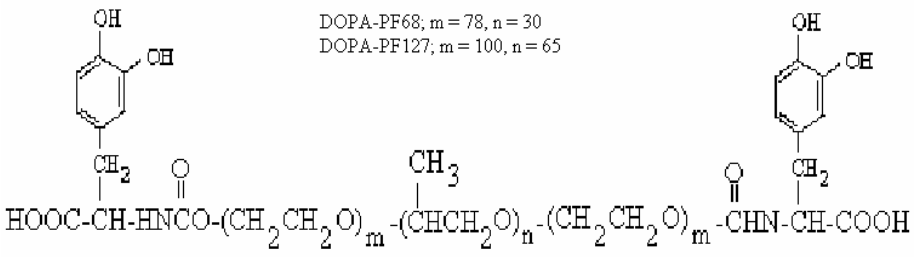

Fig. II.14. Chemical structure of DOPA-PF68 and DOPA-PF127.

III. EXPERIMENTAL

III.1. Laser ablation

Since their introduction in 1960, pulsed lasers were recognized as a flexible and powerful tool for material processing applications. In material science, laser plays a significant role either as a passive component for monitoring process or as an active tool for coupling its radiation energy into material being processed. This results in various applications such as localized melting, laser annealing, surface cleaning by desorption and ablation, surface hardening by rapid quench, pulsed laser deposition in UV and IR, and most recently, matrix assisted pulsed laser deposition (MAPLE) for growing thin films [67-70].

Lasers are unique energy sources characterized by their spectral purity, spatial and temporal coherence, and high average peak intensity. The interaction of high-power lasers with solid matter was named in various ways: vaporization, sputtering, desorption, spallation, etching or laser ablation. R. Srinivasan probably used for the first time the term of laser ablation (related to polymer ablation in 1982) which now became language [67].

The word was first used, related to lasers, to describe material removal with IR lasers. However, it has also been asserted that ablation refers to the removal of the material using UV photons where the photon energy is high enough to break atomic bonds, resulting in "cool" laser processing.

A better definition which fits all the previous examples will sound like this: the simple act of material removal by laser light can be considered "*laser ablation*" regardless of the mechanism, wavelength, pulse duration or any other factor [71].

The dynamic of laser-material interactions evidences a competition between localized and delocalized relaxation processes for the absorbed energy, as suggested schematically in Fig. III.1. Desorption of an atom or molecule can occur if the localization process wins out by retaining the absorbed energy at a single site for longer than a few vibrational periods – long enough to be broken and the atom or molecule to begin to move away from its equilibrium position [40].

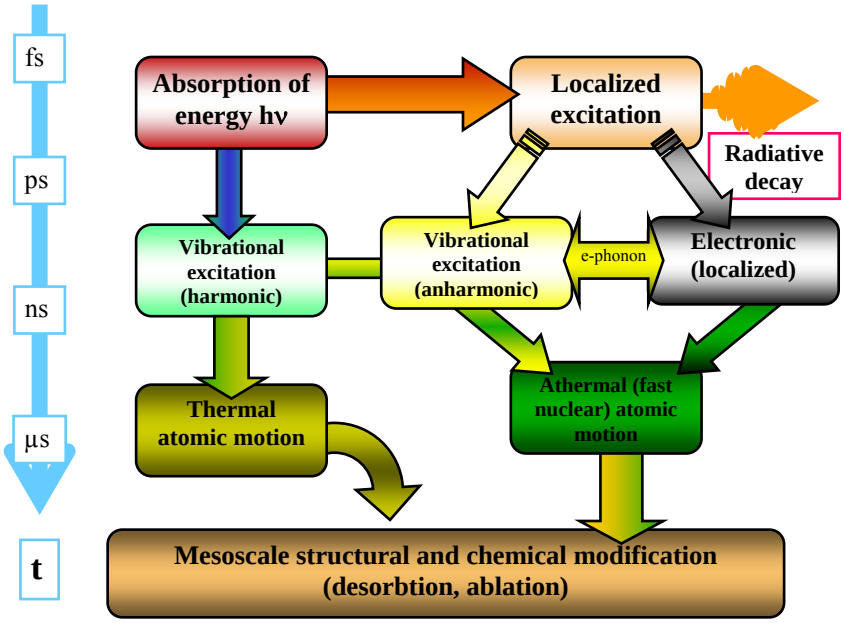

Fig.III.1. Dynamics of laser-solid interactions [40].

Radiative recombination, because of its long lifetime (typically a nanosecond or more), is actually the major channel of energy dissipation; instead, desorption and ablation processes can be viewed as one of several possible nonradiative transitions involving the following elementary energy-transformation processes:

i. electronic energy to vibrational energy by electron-phonon scattering,
ii. electronic excitation energy to configurational energy,
iii. electronic energy from one configuration coordinate to another, and/or
iv. vibrational energy from one degree of freedom to another.

If the localization condition is satisfied, one of these processes may lead to desorption or ablation. If localization does not occur at the surface, the radiationless process may simply return the system to the ground state.

The laser-induced desorption has been defined in [40] as a process for which:

i. the particle ejection without any detectable mezoscopic[1] modification of surface composition or structure,
ii. particle yield is a linear function of the density of electronic or vibrational excitation, and
iii. none of significant gas-dynamic effects is produced in the steam of particles leaving the surface.

By contrast, *laser ablation* is a process for which:

i. material removal rates typically exceed one-tenth monolayer per pulse,
ii. the surface is structurally or compositionally modified at mesoscopic length scales, and
iii. particle yields are superliniar funtions of density of excitation.

The absorption of the incident radiation by the target electrons induces localized excitations that will decay via radiative and nonradiative processes. If sufficient photonic energy is present, electronic excitation can lead directly to photochemical decomposition. More exactly, if the density of thermalized energy is above a threshold value, thermal chemistry can be observed. But there exist a regime where the thermal motion of the target species can overcome the cohesive energy of the target and surface binding energy and be desorbed. It results a vapor phase called *plume,* which can be collected to produce an adherent film. The plume formation amplifies the complexity of laser ablation due to laser-induced photochemical, gas dynamic and plasma-surface interaction processes.

III.2. Pulsed Laser Deposition (PLD)

One of the most technologically important applications of the interaction of laser light with a solid material is Pulsed Laser Deposition (PLD). The fact that a pulsed laser beam is able to readily vaporize almost any material suggested that it could be used to deposit thin films. The first demonstration of PLD dates to 1964, when Smith and Turner demonstrated the growth of thin films of various inorganic and organic materials using a ruby laser [73]. Since then, PLD has become increasingly popular within research laboratories as a method of producing thin films of novel materials.

The growth of the literature on laser ablation has been explosive. The book edited by D.B. Chrisey and G.K. Hubler [69] in 1994 makes a synthesis of fundamentals and experimental aspects of PLD and its large aplicability: from laser-material interaction and surface physics to nanostructures and biomedical applications. Ref. [74] presents the influence of deposition parameters on the performances of obtained thin films. These deposition parameters are the wavelength, pulse duration and laser fluence and energy, frequency repetition rate, target preparation, target-collector distance, substrate temperature, laser spot area, deposition geometry and nature and pressure of reactive gas in the deposition chamber. In case of gas is chemically reactive, the deposited material can have a different composition related to the target. This case is known in the literature as Reactive Pulsed Laser Deposition (RPLD). All aforementioned parameters can be controlled and varied in view of identification of the optimum regime of obtaining thin films and structures. Some aspects of laser-material interaction are analysed in the 3rd edition of the book "*Laser Processing and Chemistry"* in 2000 by D. Bauerle [75]. A special attention is payed to laser-induced chemical reactions at the gaz - solid, lichid - solid and solid – solid interfaces and to the novel developments and limits of laser processing.

Conceptually and experimentally, PLD is an extremely simple thin film deposition technique. It consists of a target holder and a substrate holder housed in a vacuum chamber as schematically shown in Fig. III.2.

[1] The term "mesoscopic physics" was coined by the Dutch physicist Nico van Kampen in Ref. [72]. It obviously broadly refers to systems which are somewhere in between macroscopic (i.e. classical) and microscopic (i.e. quantum, atomic or subatomic) systems. Accordingly, the realm of mesoscopic physics is defined by systems which are coherent, i.e. whose (dynamical, transport or equilibrium also) properties derive from and can be described by quantum mechanics.

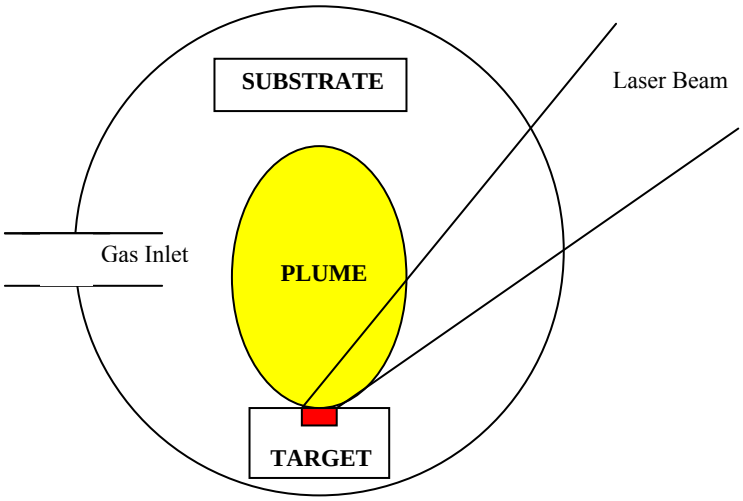

Fig. III.2. Schematic diagram of PLD.

PLD for thin film growth offers many advantages:

i. the energy laser source resides outside the vacuum chamber, which, in contrast to vacuum-installed devices, provides a much greater degree of flexibility in materials use, geometrical arrangements, and adjustment of growth parameters;
ii. almost any material in solid form can be ablated;
iii. the pulsed nature of PLD means that film growth rates and film thickness can be controlled to a high degree;
iv. the amount of evaporated target material is localized only to that area illuminated by the laser focused spot;
v. under optimal conditions, the ratios of the elemental components of the target and film are identical, even for chemically complex systems;
vi. the kinetic energies of the ablated species lie mainly in a range that promotes surface mobility of the species upon incidence to the substrate;
vii. the ability to produce species with electronic states far from chemical equilibrium opens up the possibility to produce novel or metastable materials.

Some key parameters for PLD are:

i. The process of laser ablation has a threshold fluence which can be changed either by changing the laser pulse energy or by changing the ablation area. At fluences below the threshold only minuscule etching is observed. But when laser fluence is above the threshold the etch depth per pulse increases rapidly with increasing laser fluence.
ii. The threshold fluence depends mainly on the target material structure and target absorption coefficient at the laser wavelengths.
iii. Absorption of laser radiation causes to a temperature increase in the target material.
iv. At a certain value of laser wavelength photons had enough energy and one or two photon absorption by materials might cause direct bond cleavage in the solid, leading to rapid decomposition of the material into highly volatile molecular fragments. Usually, during transition in the plume these fragments are recombined keeping the starting material structure and in some cases even under the impact on the substrate.

III.3. Matrix Assisted Pulsed Laser Evaporation (MAPLE)

III.3.1. Why MAPLE?

Today, PLD has become a well-accepted technique for the growth of a wide variety of materials ranging from oxide ceramics to metallic alloys. It is with the oxide ceramics, though, where PLD has been most advantageous, because in addition to providing the surface of the growing film with a stoichiometric flux, it is also possible to impose an overpressure of reactive gases like oxygen. Under typical oxide ceramic PLD conditions with an incident UV laser, the interaction of the ablative vapor flux - composed of atoms, ions and small molecules - with the background gas can be used to control the film

content. When deposited on a heated substrate the constituents of the vapor flux can re-assemble into the desired phase and even the correct orientation [76].

Unfortunately for PLD, the advantages for ceramics, and inorganic materials in general, would not likely exist for the more fragile and thermally labile polymeric/organic materials [77]. Indeed, when a laser interacts with an organic target under the usual conditions for PLD, the material, which is grown in thin film form, is radically and usually irreversibly different from the starting material For example, in polymers the chemical bonds connecting loosely tethered, but very important for various applications, functional groups are often broken. The backbone organic chain is also often broken leaving the film to be made up of smaller polymeric pieces and with different functional groups terminating the ends. Changing the surface chemistry of polymeric thin films is analogous to changing the stoichiometry and thus the phase and electronic properties of inorganic thin films [69, 78-81]. Even small changes in the number of functional groups or the degree of polymerization can preclude the use of these films for their desired application. Such modifications might be acceptable for some applications, but in general the use of lasers for depositing thin films of polymeric and organic materials, requires more subtle approaches than those offered by PLD alone.

It is likely that there would be similar advantages to using a laser to physically deposit organic thin films if a suitable resolution to the aforementioned problems could be resolved. Next generation applications require tighter tolerances on the structural, morphological, and chemical composition of the thin films used in their fabrication. This is especially the case for the deposition of high quality thin films of organic or polymeric materials as opposed to purely inorganic materials where high temperatures and native oxides are used to overcome the hurdles in their fabrication. Depending on the particular application, it may be desirable to deposit films containing single or multilayer structures of different organic or polymeric materials, homogeneous composite materials, or materials with graded compositions [82]. In many situations, it will be necessary to deposit the films discretely, achieve conformal coverage, and provide high quality films, especially with regard to surface coverage uniformity and thickness control. Furthermore, there is a need for high quality organic thin films in the areas of organic electronic devices, batteries, high performance dielectrics, optical data storage, optical communications, and displays based on organic electroluminescent materials [83]. Thin films of polymeric and organic materials also might play an important role in the development of next generation microfluidic biosensors and biochips, coating drug particles with functional (drugs, polymers, smart materials) films, microneedle coatings for various therapeutic applications (vaccines, gene therapy), coatings to prevent device failure due to biofouling, and biocompatible coatings for medical implants, just to name a few. In these areas, there is a strong performance requirement that the organic thin films have structural and chemical integrity, as well as, being smooth, thin, dense, and of accurately and precisely predictable thickness [77].

When this became critical, a large-area laser-based vapor deposition technique, Matrix Assisted Pulsed Laser Evaporation (MAPLE), has been developed to deposit thin polymer films without significant decomposition [84]

MAPLE is unique because it is able to combine these attributes into one processing tool to fabricate thin films and structures unachieved by other technologies.

MAPLE technique has demonstrated the capability of transferring large molecules (molecular weight > 100 kDa) and preserving their functions. MAPLE has good thickness control, patterning capability, and a wide range of materials to choose from. It can deposit patterned films on a variety of substrate materials and geometries compatible. One important consideration in biomaterial transfer is cleanliness. MAPLE is a non-contact deposition technique, thus eliminates a major source of contamination and can be integrated with other sterile processes.

These attributes are substantiated by films and arrays of biomaterials, e.g., polymers, enzymes, proteins, antibodies, and biosensors. These materials differ from passive materials such as conductors and dielectrics in many ways, but one very important difference is that they are active, i.e., they have specific biochemical functions. These functions must be preserved after any processing. For example, a hormonal protein binds to a receptor on a cell whose function it will alter [85]. If this protein is denatured and loses its structure, it will no longer be able to bind to the cell at a specific site, i.e., it has lost its function. Denaturation can be a result of a hostile environment in terms of temperature, or radiation level. In short, biomaterial transfer requires preserving molecular functions which is a much more stringent requirement than the retention of composition in passive materials.

To preserve the function of a molecule, both the chemical composition and structure of the molecule must be preserved during processing. In addition to the form of biomaterials, their molecular size and mass are important considerations. The length scale of biomaterials can be as small as 10 nm for some proteins [85]. The molecular weight of some common proteins can be larger than 150 kDa. This means that a biomaterial transfer technique must be capable of intact transfer of molecules with sizes bigger than 10 nm and molecular weights heavier than 150 kDa to be of general application. In short, the materials requirements for a versatile biomaterial transfer technique are that they must transfer large molecules intact, and preserve the chemical structure and molecular function. The demands of device development and fabrication on a material transfer technique can vary depending on the type of device, process, and scale of production. In large-scale production, for example, a deposition technique in which multiple devices are fabricated simultaneously, a large-area vapor deposition technique is more efficient. For quick prototyping of a sensor array, however, a localized transfer technique is preferable. In addition to the materials requirement described earlier, device fabrication imposes additional constraints. Good selection of materials, thickness control, patterning, i.e., masking or lithography, and layering

ability is critical for device fabrication. The spatial resolution and accuracy for patterning will depend on the device. Some special but important considerations for biomaterial transfer techniques are they must be able to dispense a small volume of materials; compatible with different substrates materials, i.e., quartz, plastics, tissues, etc., and geometry, i.e., channels, wells, concave surface, etc.; computer aided design (CAD) computer aided manufacturing (CAM) compatible. The ability to dispense a small volume of material stems from the fact that some biomaterials are extremely expensive, i.e., some proteins (*Mytilus edulis* adhesive proteins), and in some cases only a fixed amount is available, i.e., forensic samples. The compatibility to different substrate materials and shapes allows the technique to be integrated with other technologies, i.e., microwells, microchannels, microelectromechanical (MEM) devices, etc. For prototyping, the importance of CAD/CAM compatibility cannot be overstated. Some of these aforementioned criteria for biomaterial transfer techniques are met by MAPLE.

Although the MAPLE process is similar to conventional PLD (both are vacuum-deposition techniques and they share many of the same advantages over traditional thin-film fabrication techniques) the new process has additional capabilities for depositing polymer thin films. First, the organic material arrives at the substrate surface free of solvating molecules, which eliminates solvent wetting and allows better control of coating placement. Second, the growth of multilayer structures of different compounds occurs without mixing at the layer interfaces, instead of the thin film of mixed materials that results from the solvent effects. And, unlike most traditional polymer or organic thin-film-fabrication techniques, MAPLE simultaneously deposits contamination-free films with monolayer thickness control (independent of the total thickness); requires minimal amounts of material; and provides enhanced film adhesion to the substrate. It is also easily combined with masking techniques (contact and noncontact). A unique advantage of the emerging process is that it can be easily combined with noncontact shadow masks to limit the deposition to a required area. This is useful for coating fragile substrates, such as polymer coatings on atomic force microscope cantilevers, and is less expensive and lesstime-consuming than subsequent removal by patterning and etching. Patterns of polymers and organic materials with features on a 10-μm scale have been generated by MAPLE depositions through masks. This capability is important for the manufacture of sensor arrays and electronic components, in which the desired coating area is measured in micrometers. Another advantage of the MAPLE technique is that the polymer or organic material is deposited on a substrate free of bulk solvent. In contrast, deposition techniques such as aerosol, spin, ink-jet, and dip coating require a solution of the material in a solvent to physically wet the surface of a substrate. Such techniques limit the surface choices to materials that the solvent does not dissolve. The uneven and unpredictable wetting, distribution, and evaporation of the solvent molecules result in nonuniform coatings.

MAPLE is based on the Matrix Assisted Pulsed Laser Desorption/Ionization (MALDI) mechanisms. The main difference between the MAPLE and MALDI techniques lies in the treatment of the evaporated polymer and in the selection of the matrix. In the MAPLE process, the polymer is not deliberately ionized and is collected on a substrate to form a coating rather than being directed into a mass spectrometer for further analysis [77].

III.3.2. Matrix Assisted Laser Desorption/Ionization (MALDI)

Since its beginnings in 1985, Matrix Assisted Laser Desorption/Ionization (MALDI) has developed into an effective mass spectrometric technique for large molecular weight proteins [86]. Then this method has been extended to large molecular weight polymers and biopolymers.

In MALDI, the *analyte*, in our case, polymer/biopolymer/protein, is mixed with a large excess of *matrix* material (solvent) that strongly absorbs at laser wavelength. With short, intense laser pulses, the matrix and analyte are ejected together in gas phase and accelerated into a time of flight chamber. Since the analyte does not directly absorb the energy of the laser, it generally does not undergo fragmentation.

The matrix materials used are typically organic compounds in the mass range of 100-300 Da, which absorb at the wavelength of interest.

In 1993 Fitzgerald *et al.* reported the pH influence onto 37 substitutes derivated from *pyrimidine*, *pyridine* and *benzene*. It has been noticed that all of them can be used as potential matrices for MALDI investigations of proteins and oligonucleotides [87]. New matrix – analyte combinations have been experimentally investigated and optimized [81, 88].

In 1987 Karas *et al*. discovered that the use of a matrix in laser desorption could circumvent the restrictive mass limitations of the technique [89].

Requirements of the matrix are:

i. to have a strong absorbance at the laser wavelength, and

ii. the existence of a low enough mass to be sublimable.

A low concentration of the analyte is uniformly dispersed throughout the solid or liquid matrix, deposited on the end of a probe or onto a metal plate and introduced into the pulsed laser beam.

The low concentration of analyte used has several important advantages:

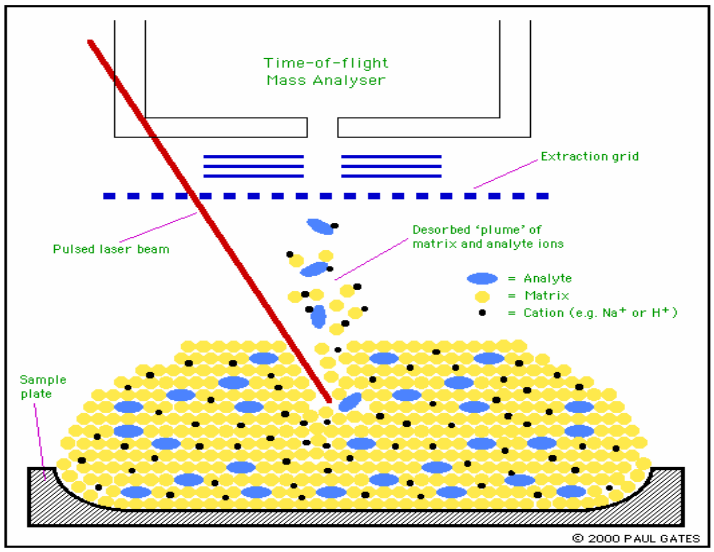

Fig. III.3. Schematic diagram of MALDI.

i. the efficiency of energy transfer from the laser to the analyte (via matrix) is increased, whereas problems associated with analyte dissociation are greatly reduced.

ii. the association of the analyte molecules to form high-mass clusters is also reduced and it is believed that suitable matrices enhance ion formation.

The mechanism of MALDI consists of three basic steps (Fig. III.3):

i. *formation of a "solid solution"*: It is essential for the matrix to be in access thus leading to the analyte molecules being completely isolated from each other.

ii. *matrix excitation*: The laser beam is focussed onto the surface of the matrix-analyte solid solution. The chromophore of the matrix couples with the laser frequency causing rapid vibrational excitation, bringing about localised disintegration of the solid solution. The clusters ejected from the surface consist of analyte molecules surrounded by matrix and salt ions. The matrix molecules evaporate away from the clusters to leave the free analyte in the gas-phase.

iii. *analyte ionisation*: The photo-excited matrix molecules are stabilised through proton transfer to the analyte. Cation attachment to the analyte is promoted during this process. Characteristic $[M+X]^+$ (X= H, Na, K etc.) analyte ions are formed. These ionization reactions occur in the first tens of nanoseconds after irradiance, and within the initial desorbing matrix/analyte plume. The ions are then extracted into the mass spectrometer for analysis.

III.3.3. Matrix Assisted Pulsed Laser Evaporation (MAPLE)

Matrix Assisted Pulsed Laser Evaporation (MAPLE) was developed at the United States Naval Research Laboratory in the late 90's for the deposition of functional organic materials (chemoselective polymers) thin and uniform layers for application in surface acoustic wave (SAW) sensors for detecting chemical warfare agents and unexploded ordinance, and in sensors developed for condition-based maintenance [4].

MAPLE is a physical vapor deposition technique capable of depositing uniform thin films over a wide area. The MAPLE instrument has four components: the pulse laser beam; the vacuum chamber; a MAPLE target mounted on a refrigerated target holder; and a substrate.

MAPLE is basically distinguished from PLD by the target preparation and significantly different laser material interaction and transfer mechanism. It provides, however, a more gentle mechanism for transferring many different compounds that include small and large molecular weight species such as sugars and polymeric molecules, from the condensed phase into the vapor phase.

Specific to MAPLE is the use of a cryogenic composite target of a dilute mixture of the polymer/biopolymer/protein to be deposited and a light absorbent, high vapor-pressure solvent matrix. Ideally, the incident laser pulse used for MAPLE initiates two photothermal processes in the matrix, evaporating the frozen composite target and releasing the polymer/biopolymer/protein into the chamber. Because of the low concentration of polymer/biopolymer/protein (1-5) wt % in the composite target, the simultaneous action of the evaporation gently desorbs the polymer or biomaterial. The photon energy absorbed by the solvent is converted to thermal energy that causes the polymer/biopolymer/protein to be heated but the solvent to vaporize. As the surface solvent molecules are evaporated into

the gas phase, polymer/biopolymer/protein molecules are exposed at the gas-target matrix interface. The polymer/biopolymer/protein molecules attain sufficient kinetic energy through collective collisions with the evaporating solvent molecules, to be transferred in gas phase. By careful optimization of the MAPLE deposition conditions (laser wavelength, repetition rate, solvent type, concentration, temperature, and background gas and gas pressure), this process can occur without any significant polymer/biopolymer/protein decomposition. The MAPLE process proceeds layer-by-layer, depleting the target of solvent and polymer/biopolymer/protein in the same concentration as the starting matrix.

Fig. III.4 shows a simplified schematic of the MAPLE desorption process and compares it to conventional PLD. Changing the target to a frozen composite modifies the laser material interaction, so that the majority of the laser energy is absorbed by the solvent molecules and not by the fragile solute. The collective action of the rapidly evaporating volatile solvent acts to softly desorb the fragile solute through soft collisions and deposits the solute as a uniform thin film whose material properties, such as chemical structure and functionality, have been maintained. Since the receiving substrate is maintained at room temperature, the sticking coefficient of the solvent is nearly zero and the evaporated solvent is rapidly pumped away. When a substrate is placed directly in the plume path, a coating starts to form from the evaporated polymer molecules.

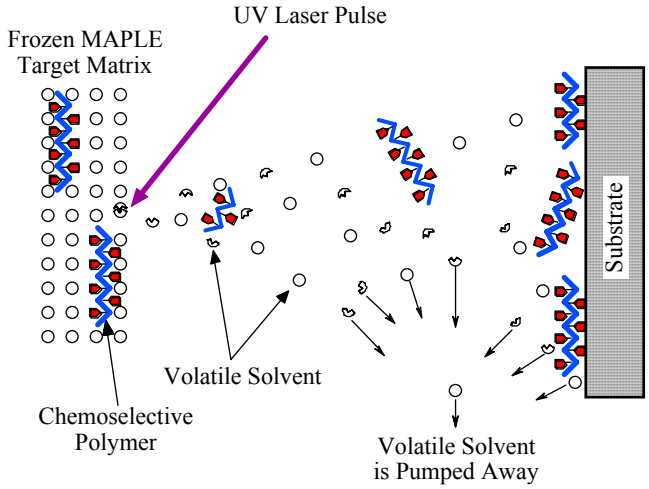

Fig. III.4. Simplified schematic of the MAPLE desorption process.

As discussed in detail by Vertes [90], the principle behind MAPLE consists of this: the molecules can survive volatilization if their liberation by disintegration precedes their destruction by fragmentation. This can be achieved by a faster heating rate, which is more likely to promote vaporization over decomposition. In this way, the adhesive/cohesive bonds between the solvent and the molecule of interest break before sufficient energy could be transferred to heat up the molecule of interest. Cold molecules can then be liberated, without damage to their structure.

Numerous studies of the pulse laser-material interactions, under similar conditions as these of MAPLE, have produced several models for the laser-solid interaction and subsequent particle emissions [91-93].

Some of these models are substantiated by experiments, which form the basis for understanding the MAPLE process [94]. Several studies have investigated the MAPLE process under different conditions such as matrix concentration, type of matrix, laser energy, and laser wavelength. The main goal of studies has been the identification of optimum conditions correspondent to each matrix – laser energy – wavelengths combination.

The original MAPLE studies were performed on polymer solutions with a specific interest toward depositing thin, homogeneous films of *fluoroalcoholpolysiloxane (*SXFA, a hydrogen bond acid functionalized polysiloxane) chemoselective polymers onto sensing platforms such as surface acoustic wave (SAW) devices in 1998 by McGill *et al.* The requirements for thin film deposition onto these devices were not being met by traditional spray coating techniques, which left large areas of film inhomogeneities due to solvent drying effects. MAPLE deposited the same chemoselective agents without solvent effects because the process is pseudodry, eliminating the solvent during deposition by performing the experiments under vacuum. To achieve the required sensor signal kinetics, it was required that the SXFA films were on the order of 10-50 nm thick and highly uniform across the whole area. In parallel to the thin film deposition, growth, and vapor testing, the electrical characteristics of the SAW sensor have been characterized [95].

Thin films of SXFA and various carbohydrates such as *glucose*, *sucrose* and *dextran* have been obtained by both PLD and MAPLE in 1999 by Pique *et al.* While PLD completely damaged the polymers, by MAPLE they have deposited high quality thin films preserving structural fidelity and uniformity [96].

The MAPLE technique has also been used to deposit composite polymer films. In 2000 Wu *et al.* successfully deposited carbon nanotubes and carbon nanotube composite thin films by MAPLE. By using this technique single-wall-nanotubes (SWN) have been transferred from the target to the substrate. The SWN sustain no observable damage during the deposition process. Using SWN in combination with *polyethylene glycol* (PEG) as a polymer matrix, SWN/polystyrene and SWN/PEG composite films were made. These films can be deposited on a variety of substrates, e.g., Si, glass, plastic, and metal, using the same target and deposition conditions. SEM micrographs show that the SWN were uniformly distributed in the film. Using a simple contact mask, SWN composite films 20 μm diameter patterns can be produced [97].

In 2001 Wu *et al.* carried out, by MAPLE, thin films of biocompatible polymers (*polyethylene glycol*, PEG), proteins and enzimes (*horseradish peroxidase*, HRP), and polyurethane composites PU/PEG and HRP. Using simple shadow masks, i.e. lines, dots and arrays, pattern features with length scales as small as 20 μm can be deposited using multiple materials on different types of substrates [98].

In 2001 Bubb *et al.* comparatively studied *PEG* thin films deposited by PLD and MAPLE onto various substrates: NaCl, Si, <111> and glass, for biomedical applications: drug delivery and *in vivo* applications. The results show that the MAPLE films nearly identically resemble the starting material, whereas the PLD films do not. These results were discussed within the context of biomedical applications such as drug delivery coatings and in vivo applications where there is a need for transfer of polymeric coatings of PEG without significant chemical modification [99].

In 2001 Ringeisen *et al.* have reported the active protein (*insulin* and *HRP*) thin films deposition by MAPLE. They put in evidence that the choice of substrate (gold, platinum, NaCl plates, hydrogenated Si, and ethylene vinyl acetate coated Si) is essential for the biomolecule adherence. MALDI, gel permeation chromatography (GPC) and electrospray ionization mass spectrometry experiments performed on MAPLE-deposited insulin films indicated that the laser-material interaction involved in this deposition technique did not modify the protein mass. FTIR spectroscopy experiments show that the chemical functionality and secondary structure of MAPLE-deposited HRP are nearly identical to those of the native protein. They also produced patterns and multilayers with feature sizes from 20 to 250 μm by depositing different biomaterials through a shadow mask. These results demonstrated that MAPLE is a preferred technique for depositing active biomolecules for applications ranging from microfluidic sensor devices to gene and protein recognition microarrays [100].

In 2002 Bubb *et al.* demonstrated that the chemical-physical properties of PEG thin films are decisively influenced by the choice of matrix: distilled water and chloroform. The photodecomposition process of the matrix occurs when using some UV wavelengths and a chloroform matrix/solvent, resulting in reactive and destructive Cl free radicals formation. These radicals are found to chemically react with solute polymers such as PEG, resulting in degraded mass distributions of the deposited film. However, with similar studies it has been shown that when a water matrix is used for PEG depositions, there are no reactive matrix species formed and molecular weight distributions are maintained when compared to the parent material [88].

Thin films of non-linear organic (NLO) materials (*N- (4-nitrophenyl)-(L)-prolinol, NPP)* conductive polymers (*polipyrrole*), luminiscent organic compounds (*8-hydroxyquinoline) aluminium*, Alq_3) and composites Alq_3/PMMA, have been obtained in 2002 by Pique *et al.* The MAPLE deposited NPP films showed optical absorptions similar to that of their bulk counterpart, while the polypyrrole films had electrical conductivities similar to polypyrrole films deposited by other techniques. In the case of the Alq3 films, the MAPLE deposited samples exhibited optical absorption patterns different from those of bulk Alq3, indicative of some decomposition that might have occurred during the MAPLE deposition process [101].

In 2003 Wu *et al.* demonstrated the MAPLE capability of transferring large molecules in different forms, e.g. liquid and gel, and preserving their function: single-wall nanotubes (SWN), biocompatible polymer (*d- ,l- lactic co-glicolid, PGA, and PLA*), patterned films (*biotinylated bovine serum albumin,* BSA) and antibiofouling coatings (*phospholipid polymer).* MAPLE is a large-area vacuum based technique suitable for coatings, i.e., antibiofouling, and MDW is a localized deposition technique capable of fast prototyping of devices, i.e., protein or tissue arrays. Both techniques have demonstrated the capability of transferring large molecules in different forms, e.g., liquid and gel, and preserving their functions. They can deposit patterned films with spatial accuracy and resolution of tens of μm and layering on a variety of substrate materials and geometries. MDW can dispense volumes less than 100 pl, transfer solid tissues, fabricate a complete device, and is computed aided design/computer aided manufacturing (CAD/CAM) compatible. These attributes are substantiated by films and arrays of biomaterials, e.g., polymers, enzymes, proteins, eucaryotic cells, and tissue, and a dopamine sensor [102].

In 2003 Fitz-Gerald *et al.* succeeded in depositing thin films of a visible light emitting polymer, [Ru*(*bpyPMMA2*)*3]*(*PF6*)*2 by MAPLE using dimethoxy-ethane (DME) as a solvent. Under a UV light the deposited materials exhibited characteristic emission at 610 nm (orange). Though a majority of the polymer seems to remain intact during deposition, proton nuclear magnetic resonance and GPC equipped with refractive index analysis reveal some polymer degradation under the conditions investigated in this preliminary study. Data are consistent with both polymer coupling reactions and some polymeric ligand dissociation from the ruthenium center [83].

Using dispersions of conductive materials, such as acetylene carbon black and non-conductive chemoselective polymers (*polyepichlorohydrin*, PECH), gas sensors based on conductimetric techniques were fabricated in 2003 by Pique *et al* [103].

In 2003 Gutierrez-Llorente *et al.* deposited *anthracene* by MAPLE using *ortho-xylene* and *chloroform* as solvents. They evidenced that the fluence value is critical in avoiding fragmentation of polymer chains. The results show that MAPLE is suitable for growing thin films of organic materials even if they absorb at the irradiating wavelength [104].

In 2004 Bubb *et al*. performed MAPLE thin films of fluoropolyol, a sorbent chemoselective oligomer. A comparison of films deposited with infrared (2.94 μm) and ultraviolet (193 nm) has been reported [105].

Toftmann *et al.* in 2004 did a comparative study of MAPLE thin films of an electroluminiscent polymer, *poly [2-methoxy-5-(2'-ethylhexyloxy)-1,4-phenylene vinylene* (MEH-PPV) conducted with two excimer lasers (193 and 248 nm) and a free electron laser (FEL) tunable in the range from 2 to 10 μm [106]. These studies highlight the potential limitations with UV MAPLE experiments and have spurred studies of the MAPLE process using less energetic wavelengths such as infrared.

In 2004 Meenakshi *et al*. deposited thin films of the molecular nanomagnet, Mn12-acetate, by MAPLE and PLD techiques. XPS shows that MAPLE films are of a superior quality as compared to those from PLD. These results open a new venue for the fabrication of arbitrarily structured thin film systems of molecular nanomagnets which allow for fundamental and applied experiments to be performed [107].

The previous examples demonstrate the capability of the MAPLE process to deposit macromolecules intact, preserve the chemical structure, transfer patterns with μm scale resolution and accuracy, and maintain functionality of the film materials. In addition, MAPLE is successful in depositing biomaterials such as enzymes and other biocompatible protective coatings [98, 100]. The integrity of most materials should be preserved in the MAPLE process with an appropriate choice of deposition parameters [108].

Thickness control in MAPLE is accomplished by simply changing the number of laser shots. For example, in the deposition of the PLGA film, the thickness is 180 nm for a total of 75,000 shots at a fluence of 165 mJ/cm^2. This corresponds to 2.4 nm/1,000 shots. Control of the thickness can be very accurate and simple in the MAPLE process. The deposition rate can also be increased by increasing the fluence or reducing the sample-to-target distance. Materials are evaporated directly from the illuminated area on the target. The illuminated area is small, ~ 5 x 10^{-6} m^2, compared to our sample size, i.e., the contact mask is 2.5 cm x 33.8 cm. The process is analogous to evaporation from a point source [91].

The MAPLE deposition rate should thus have an inverse square relationship with the distance and a power law of cos θ type angular dependence [109]. A typical deposition rate was (1.3 - 2.5) (ng/cm^2.pulse), or (1 – 2) mg in an area approximately 1 inch^2 after 40,000 laser pulses [88]. For comparison, performing UV PLD under nearly identical conditions yields a deposition rate of 10 (ng/cm^2.pulse) [99], or about 4–8 times greater than during MAPLE. Film uniformity can be improved by using a target with a larger surface area and rastering the laser beam on the target surface.

The most important consideration of the MAPLE process is to minimize photonic damage, either to the film or matrix material during laser illumination. This is because products from the decomposition of the matrix material can react with the film material. For example, Cl and HCl are produced if chloroform is used as the matrix. They can react with the film material. The factors that affect decomposition are the wavelength of the laser and the fluence. For most biomaterials, a water matrix and a 193 nm laser irradiation are used. At the fluence used for MAPLE, no decomposition of the water is found [108].

Both thermal and photonic decomposition and/or denaturation can occur. Thermal decomposition can be minimized by using lower fluences and illuminating a smaller area. This reduces the total energy deposited and a smaller heated volume. A smaller volume has a larger surface area to volume ratio, which results in a faster cooling rate and a lower maximum temperature. The photonic decomposition rate is directly proportional to the photon capture cross section for the decomposition process and the photon density or fluence. The rate can be reduced by choosing a wavelength in which the cross section is low or by reducing the photon density. The photon density can be reduced either by lowering the fluence or shielding. Surrounding the film material with a suitable matrix material can provide the necessary shielding. The MAPLE target is composed of less than 1 wt% of film material. Each film molecule is surrounded or shielded by a large amount of matrix material. This structure reduces both thermal and photonic damage to the film material [102].

Recent progress in understanding many aspects of laser ablation of organic materials has been expedited by the development of advanced computational methods and their application to various processes induced by pulsed laser irradiation. In particular, a molecular-level breathing sphere model [110], has yielded a wealth of information on the microscopic mechanisms of laser ablation, parameters of the ejected plume (velocity distributions, cluster size distributions) and their dependence on the irradiation conditions (laser fluence, pulse duration, initial temperature of the sample) [111-115]. The model assumes that each molecule (or an appropriate group of atoms) can be represented by a single particle that has the true translational degrees of freedom but an approximate internal degree of freedom. This internal (breathing) mode allows one to reproduce a realistic rate of the conversion of internal energy of the molecules excited by the laser to the translational motion of the other molecules.

To analyze the evaporation of polymer molecules in MAPLE, a molecular dynamics (MD) simulation of laser ablation where the target material was modeled as a solution of polymer molecules in a molecular matrix [116]. The breathing sphere model described above was used for MD simulations of the molecular matrix. Polymer chain molecules were described using a bead-spring model, where each bead represents one or several polymer groups. The initial stage of polymer ejection is investigated at different laser fluences and pulse durations. The influence of polymer molecules on the stability of clusters formed in the plume and the processes that can lead to polymer decomposition have been discussed. These coarse-grained models can allow a significant increase in the systém size. The objective of this study was the investigation of the effect of the laser parameters (fluence and pulse duration) on the ejection mechanisms and survivability of the polymer molecules ejected from the molecular solid. The MD simulations have showed that a result of laser excitation, polymer molecules embedded in a molecular matrix can be ejected together with the matrix material.

Two different regimes of laser ablation, stress confinement and thermal confinement, have been considered. In these regimes, the motion of the polymer molecules embedded into the matrix at different depths has been followed. The polymers are found to move faster and to start moving earlier when the laser pulse is shorter. It is shown that polymer velocities in the direction normal to the surface are not thermal and decrease exponentially with the initial depth. The calculations showed that at laser fluences above the ablation threshold, big clusters are formed in the plume. It has been demonstrated that the polymer molecules in a molecular solid tend to be located inside the clusters and stabilize the clusters as the plume expands. In addition, to reproduce the conditions realized in the developing ablated plume, a simulation of the decomposition of a laser-heated volume containing one polymer molecule has been performed. As a result of the rapid pressure built-up, the volume breaks into a number of smaller clusters. At later times, parts of the polymer molecule remain incorporated in smaller clusters that continue expanding. The main result of this study was that the polymer molecule is not fragmented during the ablation event.

III.4. Experimental setups for PLD and MAPLE

Our typical experimental setup can be described in this way: an intense laser pulse passes through an optical window in a vacuum chamber, and it is focused onto target surface. In case of the laser functional in the Laser-Plasma-Surface Interactions Laboratory, the laser pulse has a trapezoidal temporal shape, an increasing linear front of 7.5 ns, the plateau of the graph of 9 ns, and duration at the full width at half maximum of 20 ns [117].

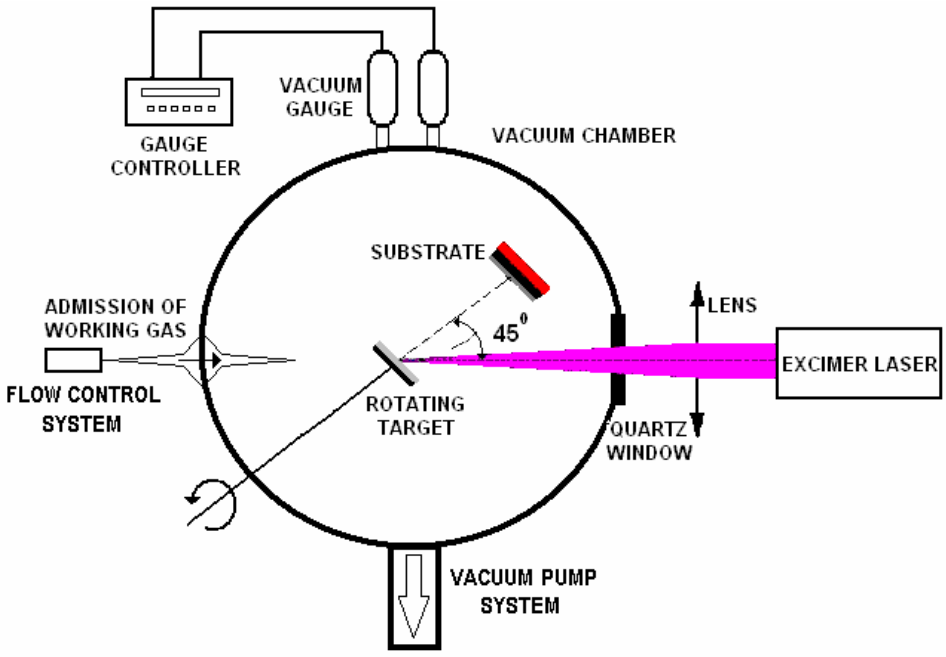

Fig. III.5. Schematic diagram of our PLD and MAPLE setups.

As visible in Fig. III.5, a typical schematic diagram of our PLD and MAPLE setups includes a vacuum chamber and a high-power laser.

Thin films and structures of PMMA, pullulan, and collagen have been obtained using a KrF* excimer laser source (λ = 248 nm, $\tau_{FWHM} \geq$ 20 ns). The laser radiation was focused by an A.R.-coated MgF_2 cylindrical lens placed outside

deposition chamber. The incident angle of the laser beam was 45°. Prior to introduction in the chamber, the substrates were cleaned with ethanol and acetone, respectively, for 10 minutes in an ultrasonic bath. The target was rotated at 0.4 Hz during the PLD process in order to avoid drilling. To mentain a constant dynamic pressure inside the chamber a MKSP400 flowmeter was used.

Thin films and structures of *Mytilus edulis* adhesive protein analogs, DOPA-PF68 and DOPA-PF127 have been deposited with an ArF* excimer laser (λ = 193 nm, τ_{FWHM} = 30 ns) operated at 20 Hz. During deposition the target was rotated at 0.4 Hz and kept at ~ 173 K using copper braids connected to a liquid nitrogen reservoir to provide the cooling.

The substrates used in MAPLE experiments were of silicon (100) (cleaned with methanol) and NaCl slides (blown dry using a nitrogen gas gun). The chamber was first evacuated down to a residual pressure of less than 10^{-5} Pa. During depositions the pressure rises to no greater than 10^{-4} Pa due to the laser-induced desorption. The target – substrate distance was of 70 mm.

MAPLE technique is applied using the same PLD experimental setup (Fig. III.5) excepting that the laser beam is focused onto a cryogenic composite target.

III.5. PLD and MAPLE studies

The following sets of experiments are reported in this thesis:

a. PLD of PMMA;
b. PLD of pullulan;
c. MAPLE of pullulan;
d. MAPLE of collagen;
e. MAPLE of *Mytilus edulis* adhesive protein analogs: DOPA-PF68 and DOPA-PF127.

III.5.1. Target preparation

III.5.1.1. PLD pressed targets of PMMA and pullulan

PMMA targets used for PLD experiments were pellets with 15x15x2 mm^3 dimensions manufactured from high purity ICI DIAKON powder by melting at 190°C.

Pullulan targets for PLD were (30x30x3) mm^3 pellets manufactured from high purity pullulan powder by pressing at $5x10^5$ Pa.

III.5.1.2. MAPLE cryogenic composite targets of pullulan, collagen and *Mytilus edulis* adhesive proteins analogs

In MAPLE, a frozen matrix consisting of a dilute solution of a polymeric compound in a relatively volatile solvent is used as the laser target. The solvent and concentration are selected so that:

i. the solute, in our case, polymer, biopolymer or protein, can dissolve to form a dilute, particulate free solution,
ii. the most of the laser energy is initially absorbed by the solvent molecules and not by the solute molecules, and
iii. there is no photochemical reaction between solvent and solute.

The solutions containing pullulan, collagen or *Mytilus edulis* adhesive protein analogs were carefully mixed at room temperature and, in case of pullulan and collagen, subsequently filtered through G_3 - type porous glasses membranes. They were prepared by dissolving pullulan in glycerol, ethylene glycol, tert butanol, dimethyl sulfoxide. Pullulan, collagen and *Mytilus edulis* adhesive protein analogs were dissolved in distilled water. The resulted solution was put in a stainless steel cup with the size of target 3 cm diameter and 5 mm height. The solution was then frozen at 77 K by immersion in liquid nitrogen and/or maintained in direct contact with a cooler [102]. This way the rapid target evaporation is slowed down. The target and the substrate were placed inside irradiation chamber at a distance set within the range (1 – 10) cm. During MAPLE depositions of pullulan and collagen a (15 – 20) Pa high purity Nitrogen flux circulated through chamber. In case of *Mytilus edulis* adhesive protein analogs the pressure rises to no greater than 10^{-4} Pa.

III.5.2. Laser processing parameters of polymers, biopolymers and proteins

III.5.2.1. PLD of PMMA

Structures and thin films from PMMA bulk have been obtained by PLD [80] using a maximum output energy of 85 mJ/pulse and a frequency repetition rate of 1 Hz. The laser spot area was set within the range of (4.2 – 6.4) mm^2. The incident laser fluence was varied from 0.8 to 1.6 J/cm^2. A heating device was used in order to keep the deposition substrate at a pre-selected temperature within the range (25 - 200) ^oC.

The investigated PMMA samples are presented in Table III.1.

Table III.1. PLD experimental conditions of structures and thin films of PMMA.

Sample symbol (Fig. IV.2, IV.4 & IV.6)	Substrate	T(^oC)	Laser fluence (J/cm^2)	Number of pulses	Film thickness in center (μm)	Film thickness at border (μm)
F1	silicon	room temperature	1.4	30000	14	20
F2	silicon	200	0.8	20000	9	14
F3	silicon	200	1.2	10000	4	6
PMMA_PLD	quartz	room temperature	1.7	30000	16	22
PMMA_PLD 400^{o}C Ar	quartz	annealed at 400 ^{o}C in Argon flow	-	-	-	-

III.5.2.2. PLD of pullulan

Structures and thin films from pullulan have been obtained by PLD [81] at (1 - 2) $x10^{-3}$ Pa. After preliminary tests, we set the incident laser fluence at a value within the interval of (210 - 570) mJ/cm^2. We used between 20,000 and 25,000 pulses. A frequency repetition rate was set at 2 Hz. During deposition the collectors were kept at room temperature. The laser spot area was chosen within the range of (0.14 - 0.29) cm^2.

The deposition conditions are summarized in Table III.2.

Table III.2. PLD experimental conditions of structures and thin films of pullulan.

Sample (FTIR spectrum symbol Fig. IV.8)	Residual evacuation pressure [$x10^{-3}$ Pa]	Energy/pulse [mJ]	Spot area [cm^2]	Incident fluence [mJ/cm^2]	Number of applied subsequent laser shots
PLD 1 (c)	1	80	0.14	570	25,000
PLD 2 (d)	2	55	0.14	390	20,000
PLD 3 (e)	2	60	0.23	260	20,000
PLD 4* (-)	2	60	0.29	210	20,000

*No deposition ($\Phi \leq \Phi_{th}$), as revealed by visual inspection and FTIR studies.

III.5.2.3. MAPLE of pullulan

Structures and thin films from pullulan have been obtained by MAPLE [81]. The colloidal solution containing less 2% pullulan was carefully mixed and then frozen at 77 K. The solvents tested in MAPLE experiments are listed in Table III.3.

Table III.3. Chemical formula and melting point for solvents used in MAPLE of pullulan.

Solvent	**Chemical formula**	**Melting point [K]**
Water	H_2O	273
Ethylene glycol	$HOCH_2CH_2OH$	260
Ethanol	CH_3CH_2OH	159
Tert-buthanol	$(CH_3)_3COH$	298
Dymethyl sulfoxide	$(CH_3)_2SO$	291.5

Depositions using ethylene glycol as solvent failed because of swelling and melting after an incomplete irradiation cycle. The target flowed after no more than 3,000 subsequent laser pulses and the obtained structures were too thin for reliable characterization. Furthermore, the frozen ethanol targets melted even before the circulation of low pressure Nitrogen was established. Further investigations were continued with distilled water, tert-butanol or dimethyl sulfoxide as solvents.

The incident fluence was set at values slightly surpassing the ablation threshold fluence of 230 mJ/cm^2 for every particular solvent. The irradiation spot area was set appropriate by within the range (0.06 - 0.27) cm^2. The number of subsequent pulses applied for a deposition of one film was (3,000 – 10,700). The adequate MAPLE deposition conditions are summarized in Table III.4.

Table III.4. MAPLE experimental conditions of structures and thin films of pullulan.

Sample (FTIR spectrum symbol Fig. IV.9.)	Solution	N_2 pressure [Pa]	Number of applied subsequent laser shots	Energy/pulse [mJ]	Spot area [mm^2]	Incident fluence [mJ/cm^2]
MAPLE1 -	2% pullulan in distilled water	18	7,000	20	1.2	163
MAPLE2 (b)	2% pullulan in distilled water	20	10,700	15	0.6	240
MAPLE3 -	2% pullulan in ethylene glycol	20	3,000	50	2	240
MAPLE4 -	2% pullulan in ethanol	-	-	-	-	-
MAPLE5 (c)	2% pullulan in tert-butanol	20	5,000	65	2.7	240
MAPLE6 (d)	Filtered 2% pullulan in tert-butanol	15	6,000	55	2.3	240
MAPLE7 (e)	Filtered 2% pullulan in dimethyl sulfoxide	15	7,000	55	2.4	230

III.5.2.4. MAPLE of collagen

The biopolymer investigated in this thesis is the high quality type I fibrilar collagen [46]. Structures and thin films from collagen have been obtained by MAPLE [118] at a frequency repetition rate of 3 Hz. The target – substrate distance was set at 3 cm. After preliminary tests, we set the incident laser energy at a value within the range (20 - 35) mJ. The laser spot area was (3.5 – 18.5) mm^2. The number of subsequent pulses applied for the deposition of one film was 10,000. All MAPLE deposition conditions are listed in Table III.5.

Table III.5. MAPLE experimental conditions of structures and thin films of collagen.

FTIR spectrum symbol (Fig. IV.14)	N_2 pressure [Pa]	Energy/pulse [mJ]	Spot area [mm^2]	Incident energy / spot area [mJ/cm^2]
a	19	20	3.3	600
b	16	35	7.4	475
c	19	30	10	300
d	19	30	18.5	160

III.5.2.5. MAPLE of *Mytilus edulis* adhesive protein analogs

The mussel adhesive protein analogs were prepared 2% concentration solutions by dissolving the DOPA-PF68 and DOPA-FP127 in distilled water at room temperature [119]. DOPA-PF68 and DOPA-PF127 [66] are L-DOPA modified-PEO-PPO-PEO block copolymers. This solution was introduced in an aluminum target holder having 20 mm diameter and 4

mm height and frozen in liquid nitrogen. The target – substrate distance was maintained at 70 mm. During deposition the target was rotated at 0.4 Hz and kept at ~ 173 K using copper braids connected to a liquid nitrogen reservoir to provide the cooling. After preliminary tests, the incident laser energy was maintained within the range of (10.2 – 21.7) mJ. The laser spot area was set within the range of (2.5 – 3.5) mm^2. The number of subsequent pulses applied for the deposition of one film was of 25,000 – 57,000. The deposition conditions are given in Table III.6.

Table III.6. MAPLE experimental conditions of structures and thin films of Mytilus edulis *mussel adhesive protein analogs: DOPA-PF68 and DOPA-PF127.*

Sample	Solution	Substrate	Number of laser shots	Energy/pulse [mJ]	Spot area [mm^2]	Incident fluence [mJ/cm^2]
1	2% PF68-DOPA in distilled water	Si	25,000	0.01025	2.5	401
2	2% PF127-DOPA in distilled water	Si	25,000	0.01025	2.5	410
3	2% PF68-DOPA in distilled water	NaCl	57,000	0.0217	3.5	620
4	2% PF127-DOPA in distilled water	NaCl	50,000	0.0217	3.5	620

III.6. Investigation methods and devices

The obtained thin films and structures have been investigated from the point of view of :

i. *crystalline state* by *X-Ray Diffraction* (XRD),
ii. *chemical composition* by *X-Ray Photoelectron Spectroscopy* (XPS), *Fourier Transform Infrared Spectroscopy* (FTIR) and *Raman Spectroscopy*, and
iii. *surface morphology* by *Optical Microscopy* (OM), *IR - Scope*, *Atomic Force Microscopy* (AFM), *Scaning Electron Microscopy* (SEM) and *High Resolution Transversal Electron Microscopy* (HRTEM).
iv. *surface adherence* by contact angle measurements.

XRD: XRD patterns of the PMMA thin films and structures were recorded using a computer-controlled TUR M-62 diffractometer equipped with a copper target tube and a proportional counter. The diagrams were obtained by recording the scattered X-ray quanta in the $(2\text{-}24)^o$ theta range with an angular step of 0.05^o (θ). The counting time was of 10 seconds per point.

XPS: XPS investigations of the PMMA deposited films have been performed with an ESCALAB MK II (V. G. Scientific) spectrometer. XPS data of the *Mytilus edulis* adhesive protein analog thin films were acquired using a Surface Science Laboratories Model SSX-100 Small Spot ESCA Spectrometer containing a monochromatized Al K-alpha X-ray source. An electron gun SPI Model 9602 True Spot was used to control specimen charging. Spectra were collected for a 400-800 μm diameter X-ray spot size using a spectrometer band pass energy of 50 – 150 eV.

FTIR: The FTIR spectra of PMMA thin films and structures were recorded with a Nicollet AVATAR 320 apparatus with a resolution of 4 cm^{-1}. FTIR spectra of pullulan and collagen thin films and structures were recorded with a Thermo Nicolet Nexus apparatus with 8 cm^{-1} resolution. FTIR spectra of *Mytilus edulis* adhesive protein analogs were recorded from 4000 cm^{-1} to 600 cm^{-1} on a Bruker IFS/66 system, with 100 scan averages at 1 cm^{-1} resolution.

IR - Scope: Investigations of pullulan and collagen thin films and structures have been performed with an IR Centaurus microscope having x300 magnification and equipped with basic transmission accessories. Every spectrum was recorded after 32 scan/spectra with a resolution of 4 cm^{-1}.

Raman Spectroscopy: The Raman spectra of PMMA thin films and structures were recorded with an Ocean Optics R-2001 instrument. A GaAs laser diode of 500 mW power was used for illumination.

MO: The Optical Microscopy investigations of pullulan thin films and structures have been done by an Carl Zeiss NU2 instrument equipped with an EPSON CCD camera.

AFM: The AFM measurements of PMMA thin films and structures were conducted using a homemade built and Digital Signal Processing controlled systems. The AFM micrographs of pullulan and collagen thin films were performed with a Quesant Atomic Force Microscope with a resolution of 500 cm^{-1} at a 1 Hz scan frequency. The AFM images of *Mytilus edulis* adhesive protein analogs thin films and structures were performed using a PicoPlus atomic force microscope (Molecular Imaging, Tempe, AZ), equipped with a scanning head. This instrument provides a maximum scan range of 100 x 100 μm^2.

SEM: SEM micrographs of pullulan thin films and structures were recorded with a Japanese Electro-Optic Laboratory (JEOL) 200CX Scanning Transmission Electron Microscope (TEM-SCAN) operated at 200 kV.

HRTEM: HRTEM micrographs of collagen thin films and structures were recorded on a 2000 Philips Customized Microscope 120 Super Twin (CM120ST).

Profilometry: The thickness of the PMMA thin films and structures has been measured using a Talysure Taylor-Hobson profilometer.

Contact angle measurements: The sessile drop method was used for contact angle measurements (Rame-Hart, Mountain Lakes, NJ). Contact angle measurements were taken at five different points for each sample, and average values were calculated.

IV. RESULTS AND DISCUSSION

IV.1. Structures and thin films obtained by PLD

IV.1.1. PMMA

We give in Fig. IV.1 the X-ray diffraction spectra of the bulk PMMA (a) and the PMMA films deposited by PLD (b-d). The PMMA bulk exhibits a typical diagram of an amorphous polymer with large diffraction maxima decreasing at high diffraction angles. The shape of the first main maximum is revealing the ordered packing of polymer chains. The intensity and shape of the second maxima are related to the effect of ordering characteristic to main chains. The films deposited at room temperature exhibit a different diffraction pattern [120]. The important modification is the narrowing of the second diffraction maximum, while the rest of the diagram shows small changes only (Fig. IV.1 b). The films deposited at 200 ^{o}C show a narrower first maximum, as compared to that of the film deposited at room temperature (Fig. IV.1 c-d).

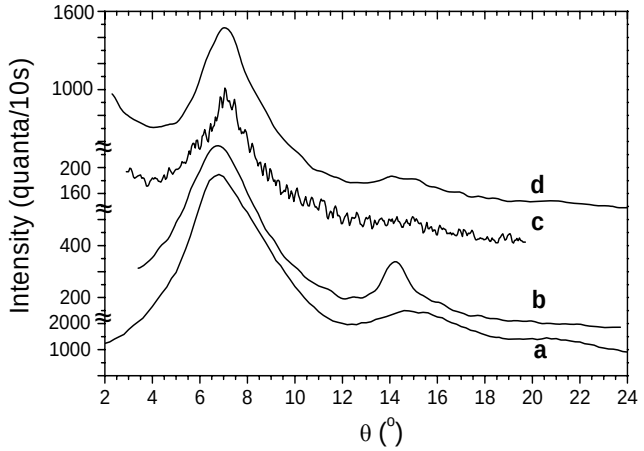

Fig. IV.1. The X-ray diffraction patterns of: (a) PMMA bulk and PMMA thin films deposited at (b) room temperature and 1.4 J/cm^2; (c) 200 ^{o}C and 0.8 J/cm^2; (d) 200 ^{o}C and 1.2 J/cm^2.

From widths of the first maximum we have calculated by the Scherer formula [121], the mean size of the ordered domains in the material, corresponding to the packing of the polymer chains. Fig. IV.2 shows the correlation between the mean size of ordered domains and the incident laser fluence on the target. The general trend is the domain increase with fluence. At room temperature, low domain values are observed.

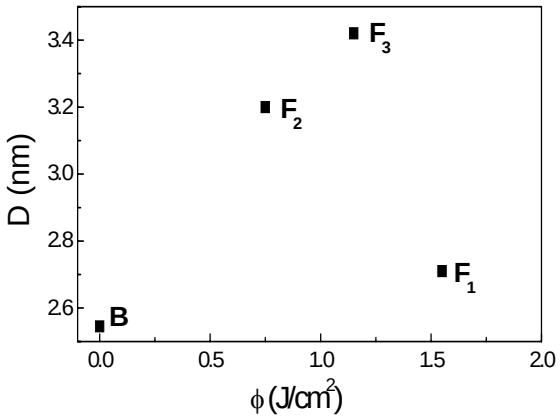

Fig. IV.2. Correlation between the mean size of ordered domains and the incident laser fluence.

XPS spectra (Fig. IV.3) provide more insight into the chemical binding in the material. The complex peak originating from the carbon 1s orbital, C1s (at 284 eV corresponding to the binding energy of the 1s electron) can be deconvoluted in three peaks. The main peak at ~284 eV is due to the C=C bonds. The second one, at ~285 eV, can be assigned to the graphite used during the preparation of XPS samples. The third one, peaking at ~288 eV is mainly due to C-O bonds in the material. The CO_2 contaminants [122] may contribute to the same peak. According to literature [123-125], the peaks located at binding energies of ~284, 285 and 288 eV are assigned to graphite, carbon from hydrocarbon configuration and diamond. The binding energies for DLC, graphite and diamond are: 1.52 - 2.63 eV, 1.12 - 1.26 eV, 1.32 - 2.81 eV. The positions and the values of the binding energy of the photoemission peak corresponding to C1s transition of carbon are in agreement with previous results of J.C. Lascovich *et al.* [126]. Higher energy component of C1s peak can be attributed to some C-O bonds. According to Ref. [122], oxygen induces a shift to higher binding energies of about 1.5 eV per C-O bond.

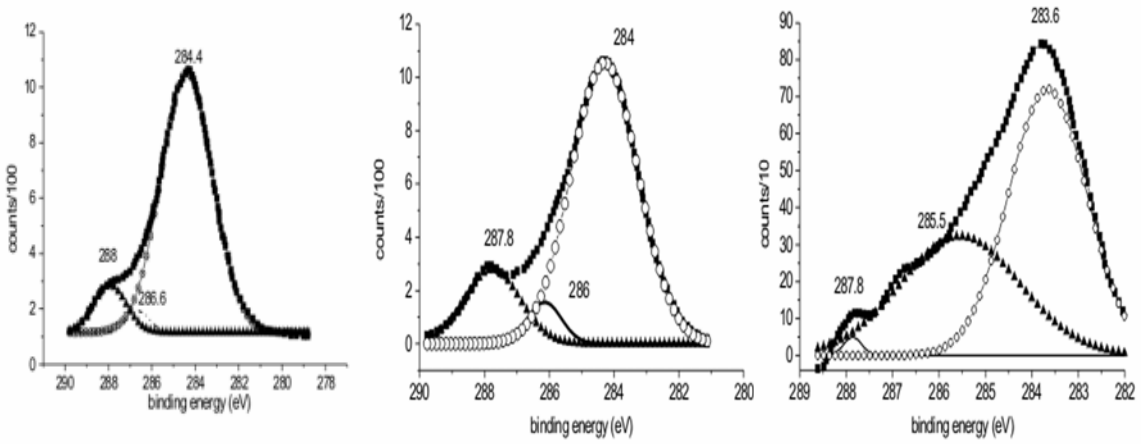

a. *b.* *c.*

Fig. IV.3. XPS spectra of: (a) PMMA bulk and PMMA thin films deposited at : (b) room temperature and 1.4 J/cm^2 ; (c) 200 ^{o}C and 1.2 J/cm^2.

We estimated the C-O contribution, by calculating the ratio of the area under the third peak ascribed to C-O bonds and that under the first peak ascribed to the C=C bonds. Fig. IV.4 shows a linear increase of the contribution of the C-O bonds in films versus the laser fluence.

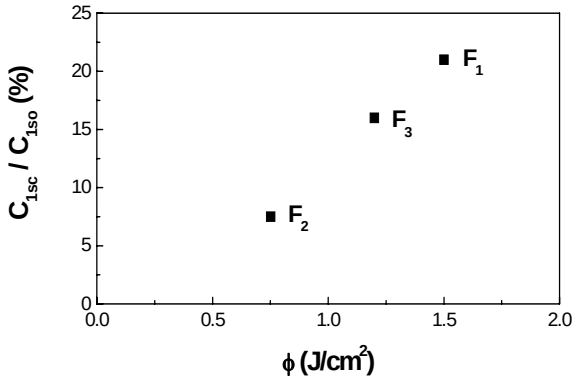

Fig. IV.4. Contribution of C-O bonds in films versus the laser fluence.

AFM studies of PMMA films deposited at 200 ^{o}C show the formation of conical protuberances (Fig. IV.5). In these zones, the film has a stratified structure, indicating a possible alignment of the molecular chains on the cone generator. The structure seems to be a-C:H like. The remaining part of the film exhibits an amorphous appearance due probably to compensate chirality [127]. For the film deposited at lower fluences (0.8 and 1.3 J/cm^2) an inhomogeneous surface is observed: dome-like structures of (15-20) nm height and (5-10) nm basis diameters. At small fluences the tendency of alignment on the cone generator keeps low. A broadening of the cones is observed. These structures are characteristic of polymers packed in spherulite-type or spiral-like configuration of packed chains. The incorporation of small spherical

particles ejected from targets during irradiation, can also account the AFM details [128]. Such configurations become possible whenever long enough chains exist in film during deposition [129-130]. The high temperature allows for a higher mobility and, therefore, a good chains package. For higher fluences (Fig. IV.5 f, Φ = 1.5 J/cm^2) the surface of films is smooth and no distinct configurations are observed.

At small fluences (0.8 J/cm^2), optical microscopy images show that films are covered with a big density of droplets. This means that the PMMA target was vaporized. The vapours condensation on substrate is preferentially taking place on specific centers (Fig. IV.5 a). We observed that these centers are mostly situated to periphery. This is the effect of the large temperature gradient on deposition surface.

The AFM image (Fig. IV.5 d) shows a unique little droplet which has a morphology with a stratified structure. This droplet is not homogenous and its formation depends on the laser fluence. Due to particle bombardament, many craters are forming and the previous morphology is modified. It visible from AFM image (Fig. IV.5 e) flattened cones are present inside craters. At very high fluences (1.5 J/cm^2), the deposition morphology is further changing (Fig. IV.5 f). The breaking of polymer chains is produced causing elimination of smaller reaction products. Simultaneously, C_xH_y structures appear. Consequently, a mixture of a-C:H and polymeric structures is ignitiated. The latter one is forming as an effect of the repolymerization of C_xH_y with liniar and breaking chains.

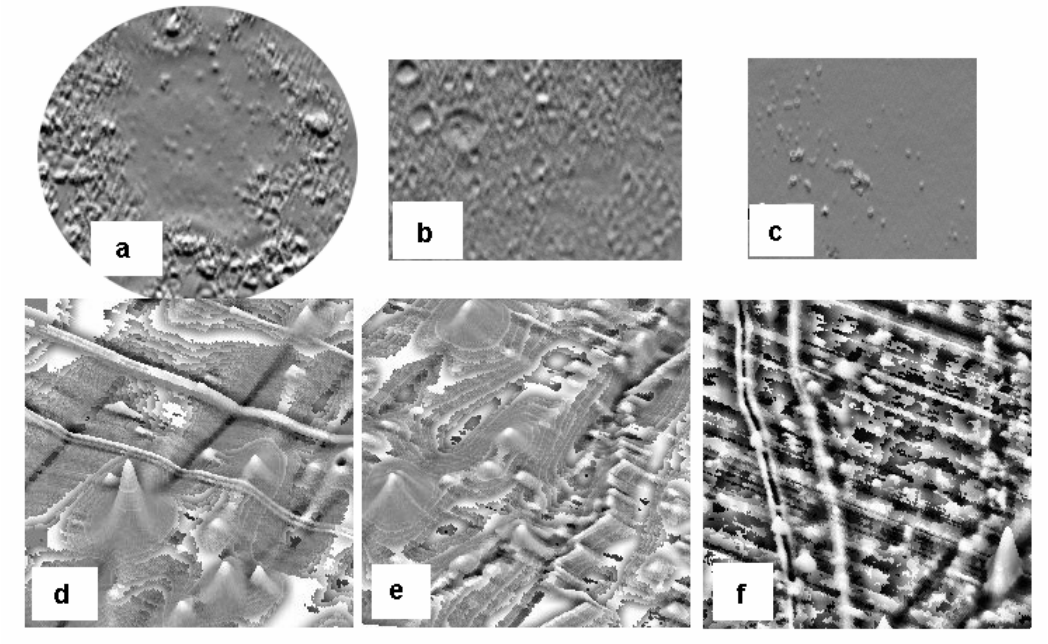

Fig. IV.5. Optical microscopy micrographs (up) of films deposited at 200 ^{o}C and : (a) 0.8 J/cm^2;(b) 1.3 J/cm^2; (c) 1.5 J/cm^2. AFM images (down) of films deposited at 200 ^{o}C and (d) 0.8 J/cm^2; (e) 1.3 J/cm^2) ; (f) 1.5 J/cm^2. In our optical microscopy and AFM photographs, the magnification is x750 and x1200, respectively.

The Raman spectra of the PMMA target and of obtained films are shown in Fig. IV.6 a-b. The spectrum of PMMA bulk shows several narrow peaks, characteristic to long folded PMMA chains. The spectra of the films look different. This is a consequence of a presence of multiple fragments and radicals in films [80]. A broad enveloping curve, mostly visible in case of F1 sample (Fig. IV.6 a), is characteristic to the diamond-like-carbon (DLC) component in film [131-133]. The Raman spectra of target, PMMA thin film obtained at room temperature and 1.7 J/cm^2, and similar film annealed after deposition at 400 ^{o}C in Ar flow are given in Fig. IV.6 b. Two peaks are relevant: the peak at 1580 cm^{-1} (1550 cm^{-1} DLC) and ~1336 cm^{-1}. As proved by the wide bell-shape of the experimental curve in the range 800 – 2000 cm^{-1}, there exists a mixture of a-C:H, DLC and aromatic chains (960 cm^{-1}). One important observation concerns the different structure of films as compared to the bulk material. These films exhibit Raman spectra of different shapes. The unusual shape of Raman spectra of F_1 film could be due to the formation of the DLC phase.

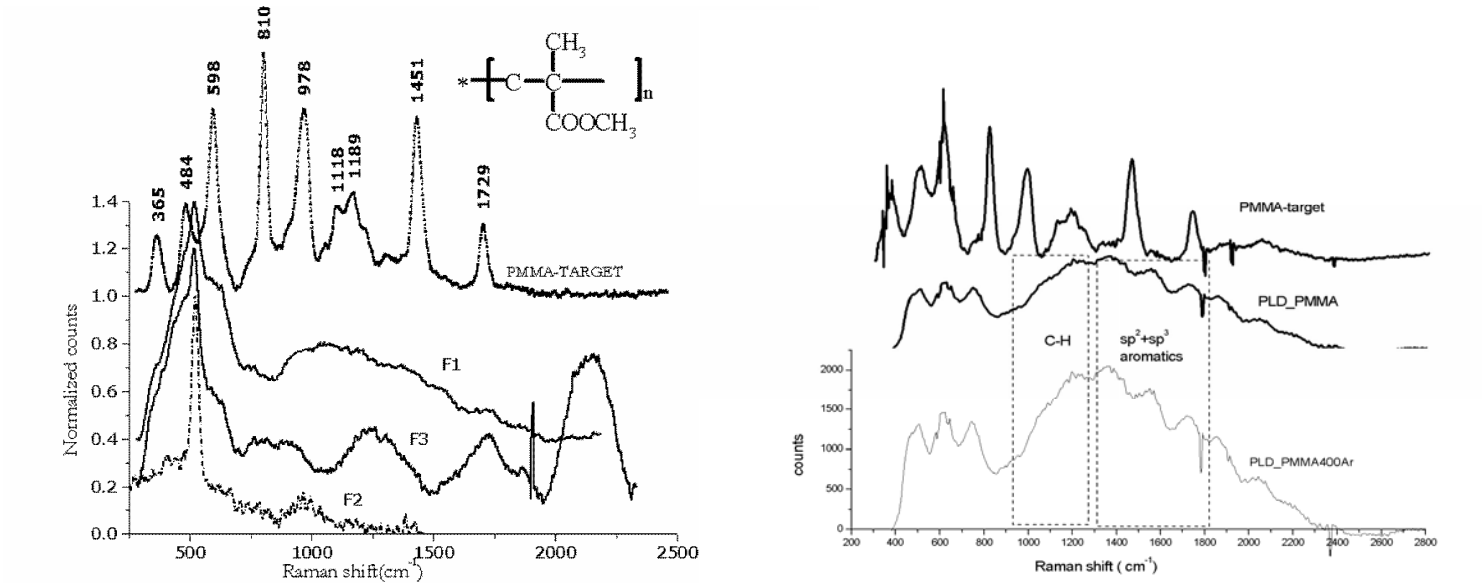

a. *b.*

Fig. IV.6. (a) Raman spectra of PMMA target (B) and PMMA thin films deposited at: room temperature and 1.4 J/cm^2(F_1), 200 ^{o}C and 0.8 J/cm^2 (F_2), 200 ^{o}C and 1.2 J/cm^2(F_3);
(b) Raman spectra of PMMA target, PMMA thin film deposited at room temperature and 1.7 J/cm^2(PLD_PMMA), and similar film annealed after deposition at 400 ^{o}C in Ar flow (PMMA_PLD400Ar).

FTIR spectra (Fig. IV.7) confirm the stable structure of DLC (a-C:H) with a high C-sp^3 abundance. To prove the correct interpretation of spectra, a sample was annealed at 400 ^{o}C in Ar in order to release the weakly bonded hydrogen. Fig. IV.7 shows an intensification of details attributed to DLC (2800-3200) cm^{-1}.

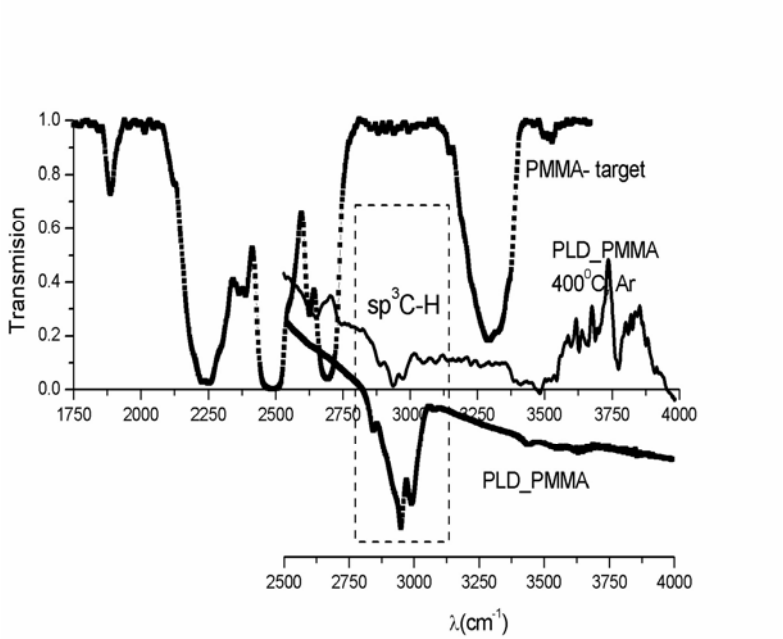

Fig. IV.7. FTIR spectra of PMMA target and PMMA thin films deposited at room temperature at 1.7 J/cm^2 (PLD_PMMA), and the similar film annealed after deposition at 400^{o}C in Ar flow (PMMA_PLD 400^{o}C Ar).

We put in evidence two phase transitions with clear thresholds. The first threshold could correspond to the modifications in the polymer structure containing a mixture of a-C:H and olefin polymers (like polyethylene, polybutadiene, etc.). The second one might be associated to the transition from a-C:H to DLC structures [127].

IV.1.2. Pullulan

We experimentally determined the ablation threshold fluence at a value of 230 mJ/cm^2.

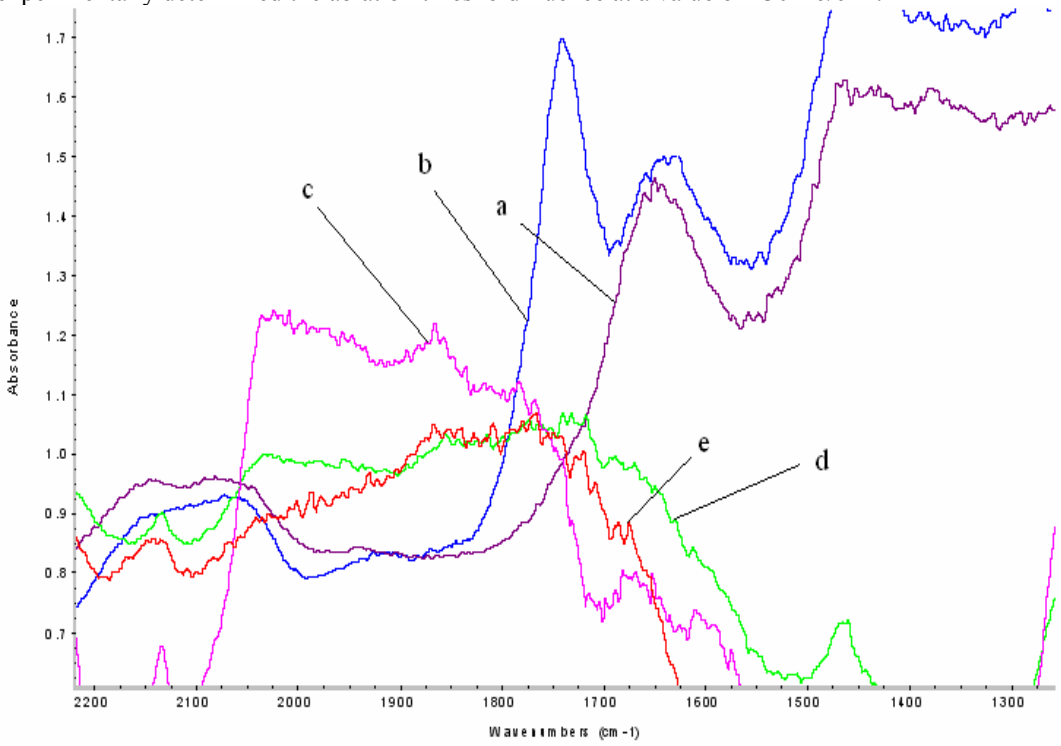

Fig. IV.8. Typical FTIR spectra in reflection for: (a) fresh pullulan target (bulk); (b) unique ring crater formed after the cumulated action of 85,000 pulses, and pullulan thin films deposited by PLD after the action of: 25,000 pulses with 570 mJ/cm^2 (c), 20,000 pulses with 390 mJ/cm^2 (d), and 20,000 pulses with 260 mJ/cm^2 (e).

In Fig. IV.8 we give typical FTIR spectra in reflection of fresh pullulan target (bulk) (a), unique ring crater formed after the cumulated action of 85,000 pulses (b), and films obtained with multipulsed laser irradiation with 25,000 pulses of 570 mJ/cm^2 (c), 20,000 pulses of 390 mJ/cm^2 (d), and 20,000 pulses of 260 mJ/cm^2 (e). The main difference between curves IV.8 a and IV.8 b is a big absorption peak present in spectrum at about ~ 1740 cm^{-1} (visible in Fig. IV.8 b). It is usually assigned to carbonyl C=O- compounds which appears from pullulan decomposition inside the crater. As it is known, in case of polysaccharides, the pyrolysis reaction leads to major chemical modifications, which generally imply water elimination or hydrocarbonate molecules breaking and carbonyl compound formation [37].

Since the spectra of obtained films and starting material are different (Fig. IV.8) we conclude that the PLD decomposes the pullulan.

One important observation is that during prolonged preservation in ambient air after deposition (several days), the obtained layers change color and gradually sublimate [81].

Consequently, we gave up making the experiments of conventional PLD from pullulan bulk target mainly because of the breaking and advanced damage of polymer chain. Under these circumstances we continued our experiments using MAPLE.

IV.2. Structures and thin films obtained by MAPLE

IV.2.1. Pullulan

In Fig. IV.9 we give typical FTIR spectra in reflection of structures and thin films of pullulan obtained by MAPLE.

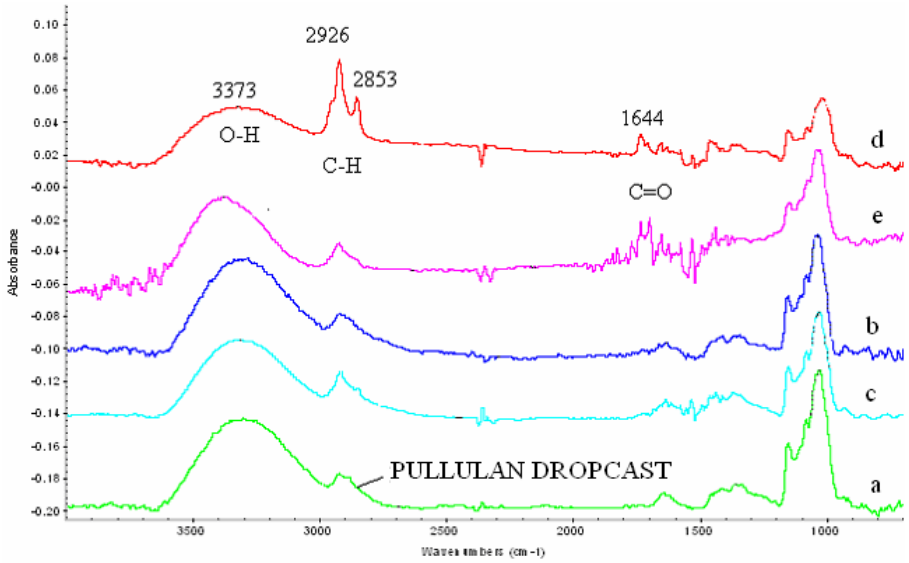

Fig. IV.9. Typical FTIR spectra in reflection for pullulan dropcast (a) and structures obtained by MAPLE from cryogenic targets of: 2% pullulan in distilled water (b, MAPLE 2), 2% pullulan in tert-butanol (c, MAPLE 5), filtered 2% pullulan in tert-butanol (d, MAPLE 6), and filtered 2% pullulan in dimethyl sulfoxide (e, MAPLE 7).

In case of a *solution of 2% pullulan in distilled water*, the reflection FTIR spectrum of thin structure (Fig. IV.9 b) is rather close to the dropcast one (Fig. IV.9 a).

Fig. IV.10 collects a sequence of images of this structure: typical SEM micrographs, AFM image and IR-scope. From SEM micrograph we note a surface containing sphere-like structures of about (3 - 6) nm diameter (Fig. IV.10 a-b). At larger magnification (Fig. IV.10 c) we observe that clusters are slightly beneath the percolation limit.

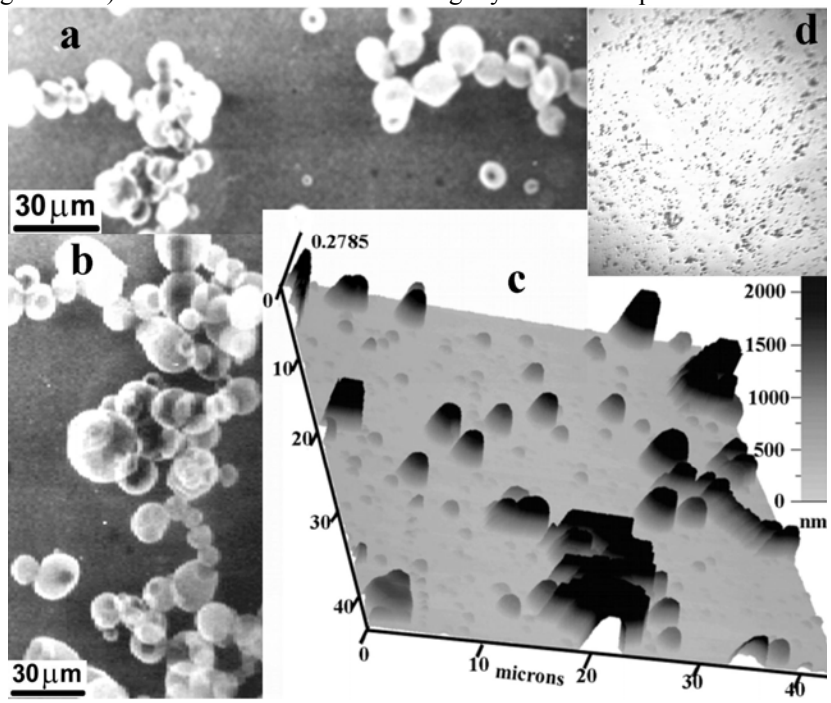

Fig. IV.10. SEM, AFM and IR-scope micrographs for structures obtained by MAPLE from cryogenic 2% pullulan in distilled water target: (a) SEM pattern, (b) high resolution details with of (a), (c) AFM image, (d) IR - scope micrograph.

This evidence is supported by AFM studies (Fig. IV.10 c). The general uniform aspect is also visible from IR-scope image (Fig. IV.10 d).

Using a *solution of 2% pullulan in tert-butanol*, we also can compare the FTIR curves in reflection of MAPLE thin structure (Fig. IV.9 c) and target (Fig. IV.9 a). We observe rather small differences. In Fig. IV.11 we give a sequence of

images characteristic to this structure. SEM micrographs exhibit a flake-like morphology with a random distribution of grains (Fig. IV.11 a-b). In our opinion, this structure can appear as an effect of a secondary Van der Waals interaction between solvent and a special transport mechanism of particulates. The IR-scope micrograph is congruent with the images pointing to a film porosity of nanometric scale (Fig. IV.11 c).

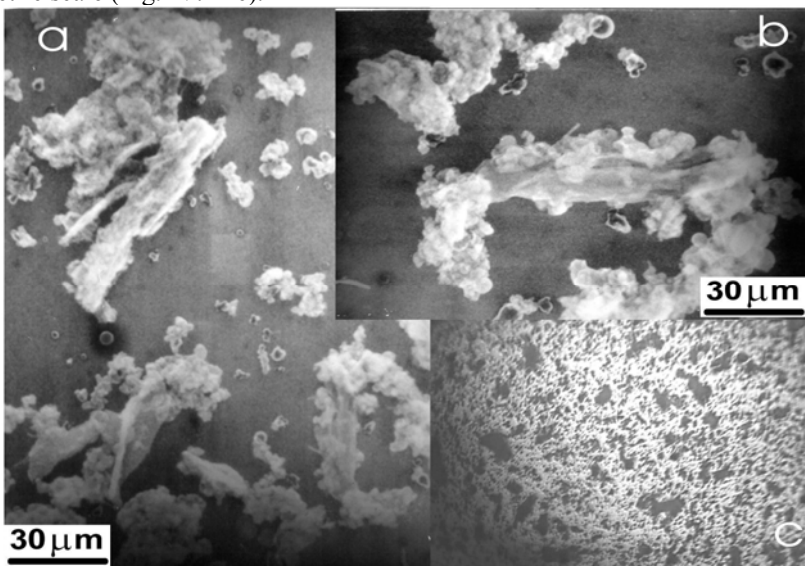

Fig. IV.11. SEM and IR-scope images for structures obtained by MAPLE using cryogenic 2% pullulan in tert-butanol target: (a) SEM pattern, (b) high resolution details of (a), (c) IR-scope micrograph.

In case of *filtered 2% pullulan in tert-butanol*, the morphology of structures and thin films is visible in SEM, AFM and IR-scope images (Fig. IV.12). The SEM micrographs exhibit a morphology consisting of islands of (1 – 4) μm particulates present either on surface or embedded into the film (Fig. IV.12 a). The AFM image (Fig. IV.12 b) shows a very smooth surface. This observation is in accordance with the IR-scope image which clearly points to island separation. It supports the idea of their deposition as particulates of different shapes and sizes (Fig. IV.12 c). The evidence in Fig. IV.12 can be corroborated with Fig. IV.9 d. In this case the deposition is produced with a mixture of pullulan and carbonyl compounds of pullulan particulates, originated, most probably, directly from the target. The carbonyl compounds are synthesized in plasma by decomposition and chemical reactions.

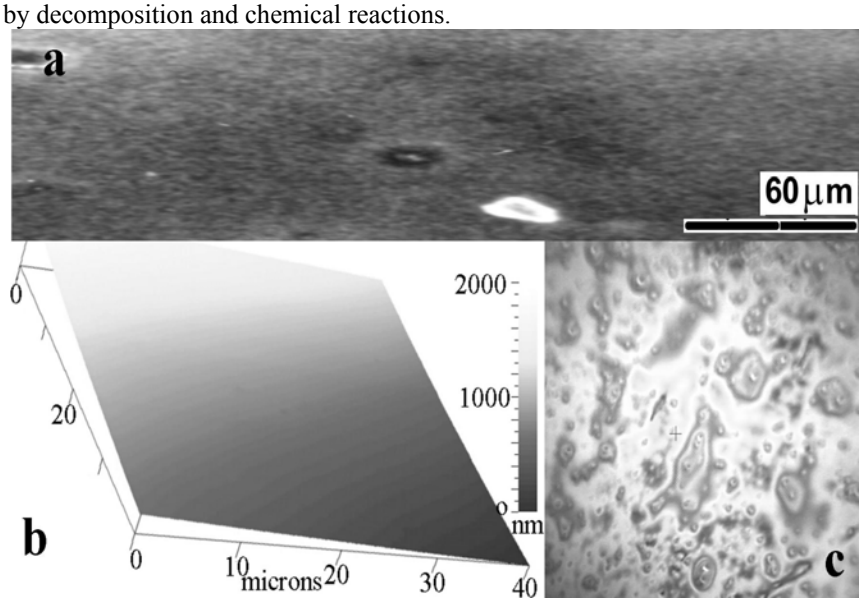

Fig. IV.12. SEM, AFM and IR - scope images for structures obtained by MAPLE for cryogenic filtered 2% pullulan in tert-butanol target: (a) high resolution SEM pattern, (b) AFM image, (c) IR-scope micrograph.

For *filtered 2% pullulan dimethyl sulfoxide*, the FTIR curve of this structure (Fig. IV.9 e) is the closest to that of target (Fig. IV.9 a). The morphology of thin film is visible in Fig. IV.13 a-c. The films appear more uniform as the previous one (Fig. IV.12) and the islands presence is less obvious.

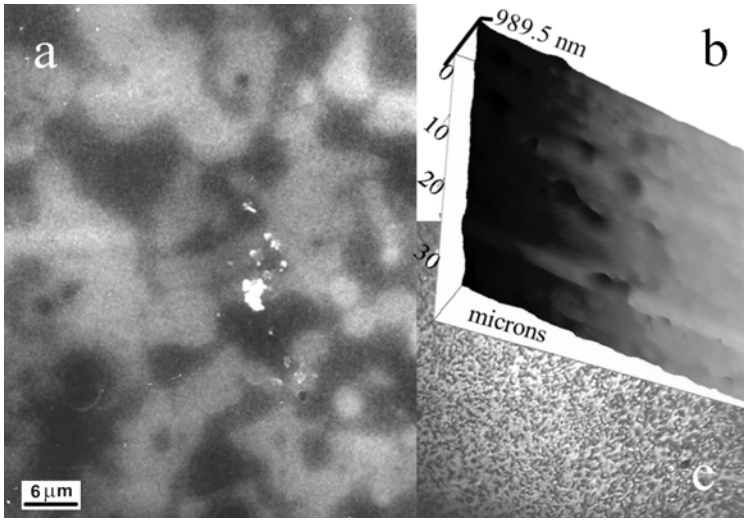

Fig. IV.13. AFM, IR-scope and SEM images for structures obtained by MAPLE using cryogenic filtered 2% pullulan in dimethyl sulfoxide target: (a) high resolution SEM pattern, (b) AFM image, (c) IR-scope micrograph.

The SEM image (Fig. IV.13 a) is in a good agreement with AFM micrograph (Fig. IV.13 b). Moreover, a microrelief with an amplitude less than 150 nm is visible in Fig. IV.13 a.

The best compromise was reached in this case between target stability and deposited thin structures performances [81].

IV.2.2. Collagen

In Fig. IV.14 we give typical FTIR spectra recorded in transmission of starting material (dropcast) and collagen thin films and structures obtained by MAPLE.

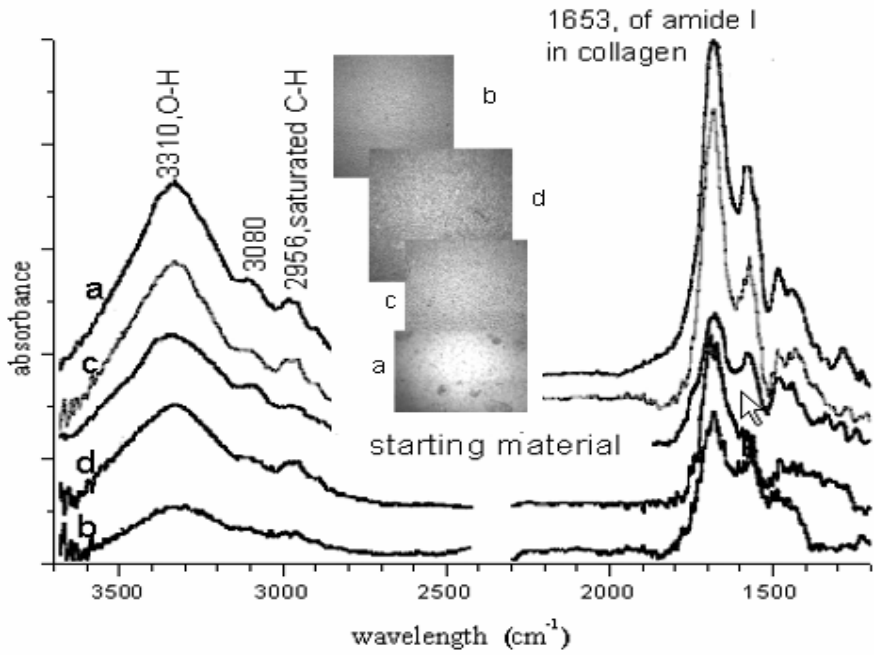

Fig. IV.14. Typical FTIR spectra in transmission and IR-scope for collagen thin films deposited at: (a) 20 mJ and 3.3 mm^2, (b) 35 mJ and 7.4 mm^2, (c) 30 mJ and 10 mm^2; (d) 30 mJ and 18.5 mm^2.

We observed no difference between the deposited thin films and reference collagen (dropcast) used in our experiments. In all our spectra four distinct bands centered at 1650 cm^{-1} (the fingerprint band for all collagens), 2950 cm^{-1} assigned to saturated C-H bounds, 3080 and 3310 cm^{-1} are visible [134]. In comparison with the dropcast, the latter two

peaks have been assigned to the two types of water molecules bound in the collagen films [118]. The intensity of these bands depends on the incident laser energy over laser spot area. These intensities are indicative for the desorption progress of water from collagen films. However, the band centered at 3500 cm^{-1} assigned to enhanced evaporation of water from collagen does not appear. More importantly, these spectra show that the main functional groups are still present on the FTIR of the transferred film, and no impurities peaks appear.

As obvious from Fig. IV.14, IR-scope images demonstrate that the homogeneity appearance is supported by the evolution of the collagen distribution from a dark appearance assigned to a less uniform collagen structure to the bright one characteristic to a more uniform one inside substrate. Therefore, the homogeneity is improving with the incident laser energy over laser spot area increase.

AFM micrographs (Fig. IV.15) present a distribution from the shape of collagen nanofibrils. It can be observed that the surface becomes smoother with the increase of the incident laser energy over laser spot area. The height of these structures is 50 nm at 20 mJ and 3.3 mm^2 (Fig. IV.15 a), increases to 200 nm at 35 mJ and 7.4 mm^2 (Fig. IV.15 b), and 400 nm at 30 mJ and 10 mm^2 (Fig. IV.15 c).

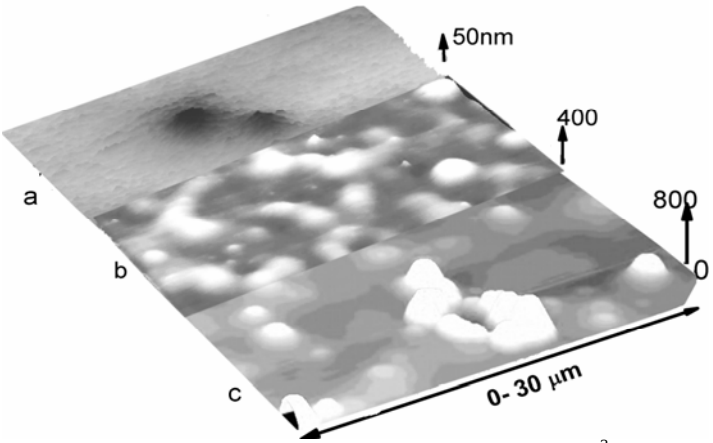

Fig. IV.15. AFM micrographs for collagen thin films deposited at: (a) 20 mJ and 3.3 mm^2, (b) 35 mJ and 7.4 mm^2, (c) 30 mJ and 10 mm^2.

Thin films show a discontinuous morphology at smaller incident laser energy over laser spot area and a continuous one noticeable in the case of higher incident laser energy over laser spot area. This can be a consequence of increasing of laser evaporated substance amount when higher incident laser energy over laser spot area is applied. Consequently, the substance incident on substrate is amplified and the film grows more uniform [118].

A typical HRTEM image recorded at an incident laser energy of 35 mJ and a laser spot area of 7.4 mm^2 is given in Fig. IV.16. We point out that this image is congruent with the corresponding AFM micrograph. The morphology of collagen nanofibrils is more evident in Fig. IV.16 a.

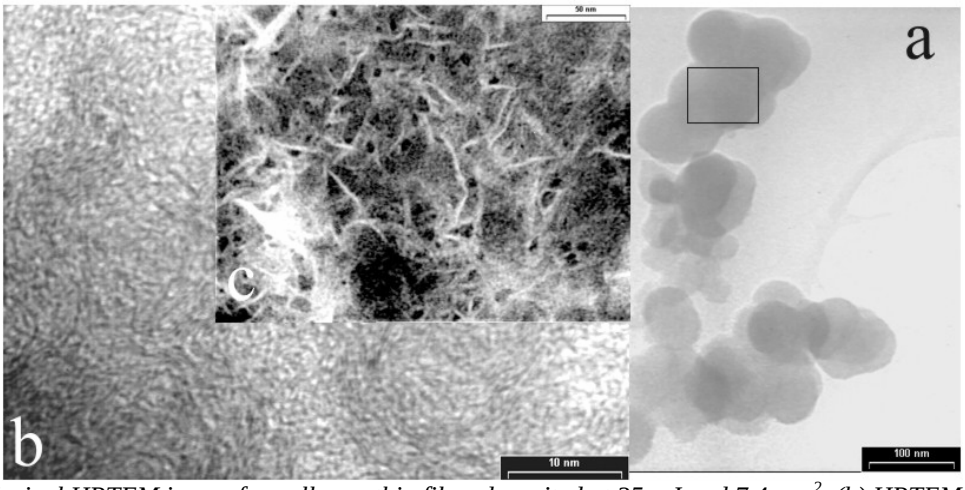

Fig. IV.16. (a) Typical HRTEM image for collagen thin films deposited at 35 mJ and 7.4 mm^2, (b) HRTEM details from (a), and (c) larger magnification detailed HRTEM from (b).

The nanofibrils are organized in cluster - like structures having a dimension of about 50 nm. In the detailed image (Fig. IV.16 c) we notice that the collagen films contain randomized long fibrils. From the more detailed picture (Fig. IV.16 b) it is evident that the mean size of fibril is 10 nm in good agreement with the available literature [135].

IV.2.3. *Mytilus edulis* adhesive protein analogs

In view of comparison between starting material and MAPLE obtained structures, films obtained by dropcasting method have been prepared [15]. At 193 nm, the deposition rate of the thin films is in the range of (0.3- 0.5) Å for every ten subsequent laser pulses [96]. The thickness of the DOPA-PF68 and DOPA-PF127 obtained films is estimated to 200 nm.

IV.2.3.1. DOPA-PF68

FTIR spectra of the MAPLE DOPA-PF68 thin films and dropcast material were recorded in transmission mode.

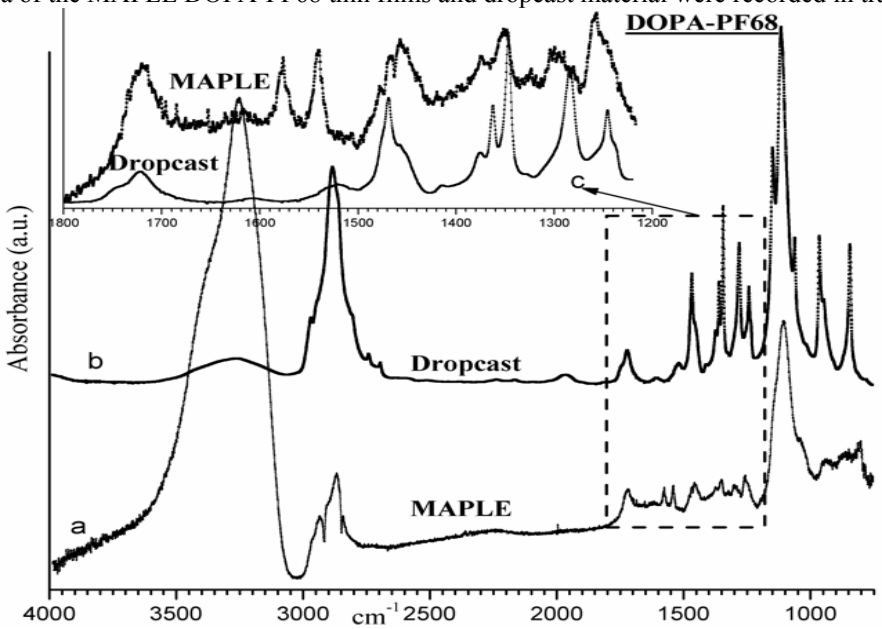

Fig. IV.17. FTIR of DOPA-PF68 Mytilus edulis *adhesive protein analog recorded in transmission mode for (a) dropcast material; (b) thin film prepared by MAPLE, with laser fluence of 620 mJ/cm^2 and laser spot area of 3.5 mm^2; (c) detailed mid-infrared spectra.*

Fig. IV.17 a contains the FTIR spectrum of the dropcast DOPA PF-68 material. Fig. IV.17 b contains the FTIR spectrum of MAPLE DOPA PF-68 thin films. The films were prepared under the following conditions: laser fluence of 620 mJ/cm^2 and laser spot area of 3.5 mm^2. Fig. IV.17 c contains detailed spectra for the dropcast material and MAPLE-deposited film in the mid-infrared range (1200 –1800) cm^{-1}.

Several distinct bands of investigated DOPA-PF68 *Mytilus edulis* adhesive protein analog are described in the literature [136-137], including those centered at 1061 cm^{-1}, 1115 cm^{-1}, 1148 cm^{-1}, 1242 cm^{-1}, 1281 cm^{-1}, 1344 cm^{-1}, 1360 cm^{-1}, 1455 cm^{-1}, 1467 cm^{-1}, 1722 cm^{-1}, 2884 cm^{-1}, and 3262 cm^{-1}. The band at 1061 cm^{-1} is assigned to C-H bending on the aromatic ring. The band at 1115 cm^{-1} is attributed to C-N stretching. The band at 1148 cm^{-1} is referred to as CH_2 wag. This band results from lateral bonds, which are secondary interactions that allow the material to form random coils. They may decrease in intensity if mobility of the lateral bonds is reduced. The band at 1242 cm^{-1} is assigned to C-O stretch from carboxylic acid. The band at 1360 cm^{-1} may result from aromatic ring deformation by substitution; this band occurs in conjunction with a weak band at 1411cm^{-1}. The band at 1455 cm^{-1} is attributed to CH_2 stretching. The band at 1467 cm^{-1} is assigned to aromatic ring stretching. This band occurs along with weak band at 1605 cm^{-1}. The band at 1722 cm^{-1} belongs to C=O stretching; and suggests that the chain configuration is preserved. The band at 2884 cm^{-1} assigned to C-H stretching suggests the chain configuration is maintained. The band centered at 3262 cm^{-1} is attributed to aromatic ring deformation by N-H stretching, and suggests the chain configuration is also preserved.

These spectra demonstrate that the main functional groups in DOPA-PF68 are present in the MAPLE-obtained film. There are bands at 1652 cm^{-1}, 1576 cm^{-1}, and 1540 cm^{-1} that appear in MAPLE-obtained films and not in dropcast films. These three bands do appear in a reference spectrum of L-DOPA taken with a KBr pellet. The MAPLE-obtained films influence the conformation of the repeating polymer units by increasing entropy and increasing the number of random coils. A slight shift in the main bands that appear in the FTIR spectra of DOPA-PF68 could be due to the conformational

modifications of macromolecules during the films deposition. Overall, good agreement is observed between absorption bands of MAPLE-obtained thin films and dropcast DOPA-PF68 reference material.

Fig. IV.18 a gives an AFM micrograph of mussel adhesive protein analog DOPA-PF68 thin film prepared by MAPLE, with laser fluence of 410 mJ/cm^2 and spot area of 2.5 mm^2. Fig. IV.18 b contains AFM detail of Fig. IV.18 a at 10 μm scale, and Fig. IV.18 c presents embossed flattened detail image of (b) at 3 μm scale. Fig. IV.18 a demonstrates that the surface of this film consists of ripple-like structures. The height of these structures is about 100 nm. A network of almost oriented distributed roped chains can be observed on each ripple. As seen in Fig. IV.18 c, these chains possess an average width of 200 nm. They are separated by zones of about 100 nm width. The presence of these structures suggests that the DOPA-PF68 thin film exhibits a randomized coiled polymer configuration.

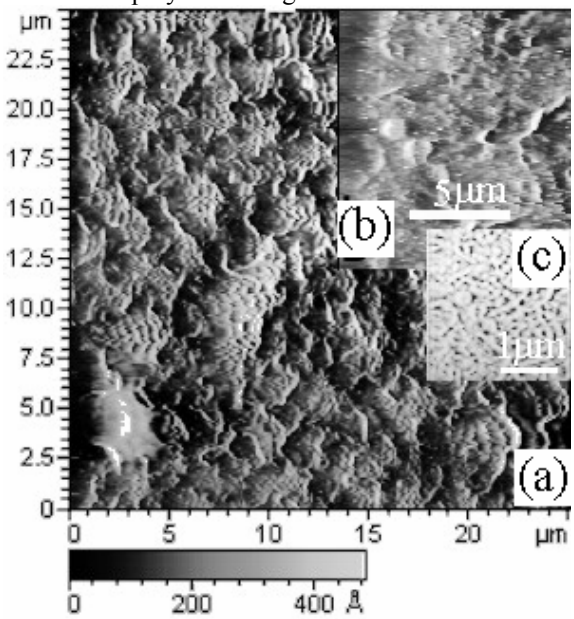

Fig. IV.18. (a) AFM micrograph of DOPA-PF68 Mytilus edulis *adhesive protein analog thin film prepared by MAPLE at 410 mJ/cm^2 and 2.5 mm^2, (b) AFM detail of (a), (c) embossed flattened detail image of (b).*

IV.2.3.2. DOPA-PF127

FTIR spectra of the MAPLE obtained DOPA-PF127 thin films and the dropcast materials were recorded in transmission mode (Fig. IV.19). We expect a more enhanced reptation tendency [138], because DOPA-PF127 chain is longer and more flexible than DOPA-PF68. The MAPLE-obtained thin film and the dropcast material contain distinct bands centered at the same wavenumbers. The band intensities within the range (242 – 1467) cm^{-1} are decreased in the MAPLE-obtained thin film when compared to the dropcast material. This result suggests an increased tendency of reptation, increased entropy, and conformational repeating polymer unit transformation in the MAPLE DOPA-PF127 film. The MAPLE DOPA-PF127 film and the dropcast material exhibit similar bands in the region within the range (1722 – 3262) cm^{-1}. Overall, a good agreement is observed between absorption bands of MAPLE-obtained thin films and dropcast material. MAPLE is well-suited for DOPA-PF127 transfer, because the chemical structure of the transferred material is well preserved [119].

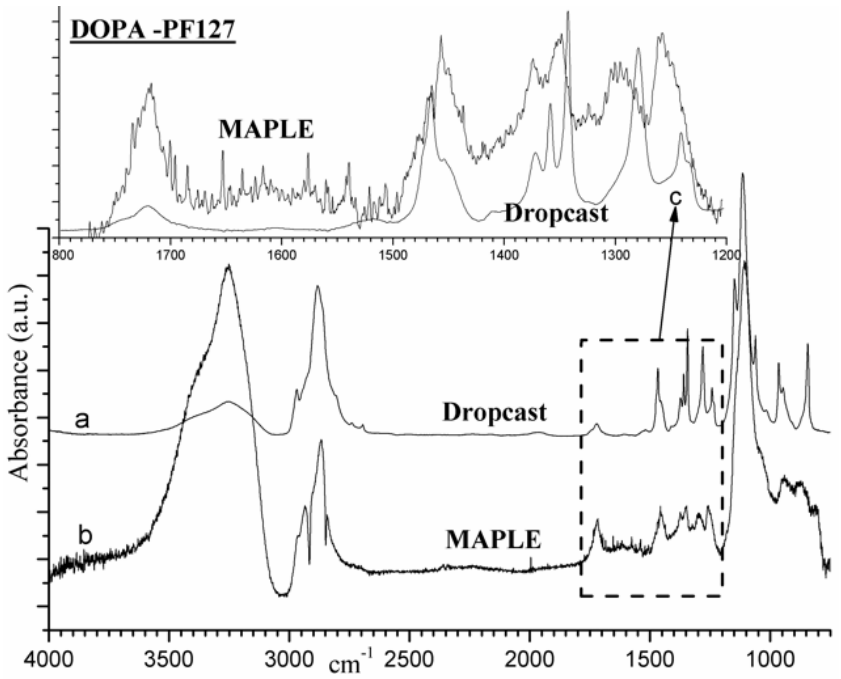

Fig. IV.19. FTIR spectra of DOPA-PF127 Mytilus edulis *adhesive protein analog recorded in transmission mode for (a) dropcast material; (b) thin film prepared by MAPLE at 620 mJ/cm^2 and 3.5 mm^2; (c) detailed mid-infrared spectra.*

AFM micrograph of DOPA-PF127 thin film (Fig. IV.20) demonstrates ripple-like structures similar to those observed in Fig. IV.18. The ripples for the MAPLE DOPA-PF127 thin film are 50 nm, and are more dispersed than those observed in DOPA-PF68 thin film. These features follow from the fact that DOPA-PF127 contains a longer polymer chain length than DOPA-PF68. A network of randomized oriented roped chains is observed on each ripple; this aspect also proves that the MAPLE DOPA-PF127 film has a coiled polymer configuration. These chains have an average width of 200 nm. Uniformly distributed 100 nm diameter pores are visible between the roped chains (Fig. IV.20 c).

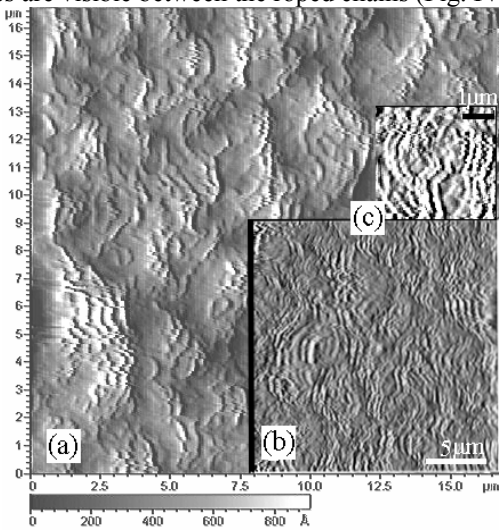

Fig. IV.20. (a) AFM DOPA-PF127 Mytilus edulis *adhesive protein analog thin film prepared by MAPLE with 410 mJ/cm^2 and 2.5 mm^2; (b) AFM details of (a); (c) embossed flattened detail image of (b).*

Fig. IV.21. contains a high-resolution XPS spectrum of C1s region of MAPLE DOPA-PF127 thin film. C1s region reveals peaks at 284.6 eV and 286.3 eV, which correspond to 38 % and 62 % of C1s bonding, respectively. The dominant C1s peak placed at a binding energy of 286.3 eV is assigned to C-N and C-O functionalities in the polymer. The peak situated at 284.6 eV is attributed to aliphatic and aromatic carbon bonds within the DOPA head groups. In addition, the hydrocarbon contamination is observed at this binding energy. The dominant chemical groups in DOPA-PF127 are the PEO-PPO-PEO groups. C-O bonds within these groups appear to provide the major contribution to the spectrum. The values quoted above are very similar to those found by other investigators [139-141].

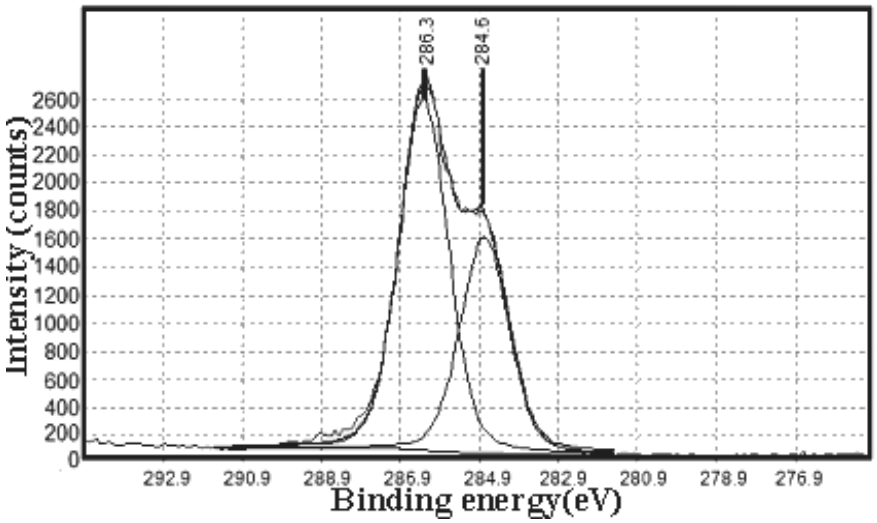

Fig. IV.21. X-ray photoelectron spectrum of the mussel adhesive protein analog DOPA-PF127 deposited by MAPLE showing peaks at 286.5 and 284.6 eV.

Contact angle testing was used to determine surface properties of MAPLE-deposited and dropcast DOPA-PF127 films. The water contact angle for the DOPA-PF127 dropcast film was 65.3˚ and 31˚ for the MAPLE-deposited film. The results observed for the MAPLE-deposited film is similar to the values reported by other investigators [142, 143].

Contact angles on polymer surfaces are influenced by surface tension, surface roughness, chemical heterogeneity, and molecular orientation. We believe that MAPLE-deposited films may contain a larger number of hydrophilic N-H groups surface than the dropcast film. For example, the FTIR spectrum for the MAPLE-deposited film contains an absorption peak corresponding to N-H stretching (3262 cm^{-1}) that is somewhat larger than that for dropcast film. In addition, previous contact angle studies have noted phase separation and heterogeneous surface formation in dropcast polymer films [144].

V. CONCLUSIONS

The main original results reported in this thesis can be sumarized in the following conclusions:

1. I have studied the chemistry of polymers (PMMA), biopolymers (pullulan), and proteins (collagen and *Mytilus edulis* adhesive protein analogs) because these biomaterials obtained as thin films and structures can offer greater versatility and cost-effectiveness than those currently available and can have remarkable biomedical applicability.

2. I have obtained thin films and structures by PLD of *PMMA*. I observed that the composition and structure of obtained films depend on laser fluence and substrate temperature. The chemical structure of thin films is different from that characteristic to starting bulk polymer. The XPS, Raman spectroscopy and FTIR investigations demonstrated that the diamond-like carbon (DLC) configuration are present in the obtained thin films and structures. The DLC abundance increases as effect of thermal postdeposition treatment at 400 ^{o}C in flux of argon.

3. I have proved that PLD technique is not suitable to obtain thin films and structures of *pullulan*. FTIR spectra have shown that obtained thin films and structures are significantly different from the bulk starting material.

4. To overcome the photochemical advanced damage I have extended experiments by implementation and development of a recent method of laser transfer known as Matrix Assisted Pulsed Laser Evaporation (MAPLE).

5. I have introduced a preparation procedure of cryogenic composite targets. I have immersed recipient containing small concentrations of polymer, biopolymer or protein, in liquid nitrogen.

6. I have proved in case of MAPLE of *pullulan* that solvent properties drastically influence composition and morfology of obtained thin films and structures. AFM and SEM investigations evidenced that films morphology evolves from sphere-like to flake-like structure. The best results have been obtained from cryogenic targets of 2% pullulan in dimethyl sulfoxide. This is the first report in literature of successful MAPLE deposition of pullulan as thin films.

7. I have shown by FTIR, AFM and HRTEM that the MAPLE of high quality purity type I collagen produced thin films and structures free of impurities, containing collagen nanofibrils. Roughness can be controlled by proper choice of deposition conditions. I have identified the best correlation between target stability during laser processing and thin films performances: uniformity, high adherence and very close structure to starting material. The distribution of collagen nanofibrils evidenced by AFM and HRTEM investigations revealed that the collagen films become more uniform and smoother when the incident laser energy over laser spot area is increased.

8. I have demonstrated by FTIR and XPS that the MAPLE of *Mytilus edulis* adhesive protein analogs, DOPA-PF68 and DOPA-PF127, is a very efficient technique that allows the growth of thin films with chemical structures identical to those of starting materials. I have examined the effect of polymer chain length upon film chemistry and morphology. AFM investigations have shown that MAPLE- deposited *Mytilus edulis* adhesive protein analog thin films exhibit a uniform distribution of ripple-like structures. As polymer chain length is increased, the roped polymer chains evolve from an oriented distribution, with almost parallel chains, to a randomized one, with uniformly distributed pores. Contact angle tests have shown that the MAPLE-deposited *Mytilus edulis* adhesive protein analog thin films have a water contact angle of 31°, in good agreement with values for L-DOPA films. These *Mytilus edulis* adhesive protein analogs have the potential to serve as adhesives in a variety of biomedical and technological applications. This is the first report in literature of successful MAPLE deposition of *Mytilus edulis* adhesive protein analogs, DOPA-PF68 and DOPA-PF127, as thin films.

9. MAPLE in its present configuration fulfills all criteria for general-purpose biomaterials (polymers, biopolymers, and proteins) transfer techniques. The specifications for this technique can easily be improved. A better optical system can improve resolution and a laser with higher repetition rates can increase speed. MAPLE increases the biomaterial selection. In addition, because the MAPLE instrument can be used for PLD, materials selection is further expanded to include all materials compatible with PLD.

10. The future development of MAPLE technique will be in three main directions: materials, devices, and instrumentation. The list of materials and their deposition parameters will be continuously diversified and refined. With an expanded list of available materials, current devices can be improved and new devices can be invented.

References

1. http://www.zyvex.com/nanotech/feynman.html.
2. I.N. Mihailescu, V. Nelea, M. Jelinek, Chapter *Hydroxylapatite and Other Ceramic Biomaterials* in: *Pulsed Laser Deposition of Thin Films: Applications in Electronics, Sensors, and Biomaterials*, edited by Douglas B. Chrisey and Robert W. Eason, J. Wiley & Sons, Spring 2005.
3. S. Vogel, MRS Bulletin June (2003) 404-408.
4. G. Koren, Appl. Phys. Lett. 50, (1987) 1030-1032.
5. S.C.K. Misra, M.K. Ram, S.S. Pandey, B.D. Malhotra, A. Chandra, Appl. Phys. Lett 60, (1992) 1219-1221.
6. S.G. Hansen, T.E. Robitaille, Appl. Phys. Lett. 52 (1), (1998) 81-83.
7. M. Sirajuddin, P.J. Reddy, Thin Solid Films 124, (1985) 149-154.
8. G.B. Blanchet, C.R. Fincher, C.L. Jackson, S.I. Shah, K.H. Gardner, Science 262, (1993) 719-721.
9. M. Shen, A.T. Bell (Eds.), ACS Symposium Series 108, American Chemical Society, Washington, DC, 1979.
10. N. Kumar, B.D. Malhotra, S. Chandra, J. Polym. Sci. C-Polym. Lett. 23, (1985) 57-61.
11. E. Sutcliffe, R.J. Srinivasan, Appl. Phys. 60, (1986) 3315-3322.
12. S. Deshmukh, E.W. Rothe, J. Appl. Phys. 66, (1989) 1370-1374.
13. S. Sun, P. Ho-Si, D.J. Harrison, Langmuir 7, (1991) 727-737.
14. I. Fujiwara, M. Ohnishi, J. Seto, Langmuir 8, (1992) 2219-2222.
15. R.A. McGill, D.B. Chrisey, *Method Of Producing A Film Coating By Matrix Assisted Pulsed Laser Deposition*, Patent No. 6,025,036, (2000).
16. E. Badarau, *Fizica Descarcarilor in Gaze*, Ed. Academiei RPR, Bucuresti, 1957.
17. I.I. Popescu, D. Ciubotaru, *Bazele Fizicii Plasmei*, Ed. Tehnica, Bucuresti, 1987.
18. I. Iova, I.I. Popescu, E.I. Toader, *Bazele Spectroscopiei Plasmei*, Ed. Stiintifica si Enciclopedica, Bucuresti, 1987.
19. I.N. Mihailescu, I. Ursu, Al. Popa, A.M. Prokhorov, V.P. Agreev, A.A. Gorbunov, V.I. Konov, J. Appl. Phys. 58, (1985), 3909.
20. A.M. Prokhorov, I. Ursu, I.N. Mihailescu, V.I. Konov, *Interaction of Laser Radiation with Metals,* Publishing House of the Romanian Academy, Bucharest, Romania, 1986 (in Romanian).
21. V. Craciun, R. Alexandrescu, I.N. Mihailescu, I. Ursu, I. Morjan, Al. Popa, M. Popescu, J. Appl. Phys. 61, (1987) 3110.
22. V. Craciun, I.N. Mihailescu, I. Ursu, F. Craciunoiu, A. Cirici, A. Luches, G. Leggieri, M. Martion, Appl. Phys. Lett. 52, (1988) 1225.
23. A.M. Prokhorov, A. Yu Bonchik, S.G. Kiyak, A.A. Manenkov, G.N. Mikhailova, A.V. Pokhmurskaya, A.S. Seferov, I. Ursu, V. Craciun, I.N. Mihailescu, Appl. Surf. Sci. 43, (1989) 340.
24. A.M. Prokhorov, I. Ursu, V.I. Konov, I.N. Mihailescu, *Laser Heating of Metals*, Adam Hilger Ltd - The Publishing House of the Institute of Physics, Bristol, England, UK, 1990.
25. V. Craciun, D. Craciun, N. Chitica, I.N. Mihailescu, M. Bertolotti, Appl. Surf. Sci. 54, (1992) 362-365.
26. A. Barborica, N. Chitica, M. Dinescu, A. Petris, I.N. Mihailescu, I. Ursu, Physica Status Solidi (a) 139, (1993) 119-127.
27. A. Barborica, N. Chitica, M. Dinescu, I.N. Mihailescu, I. Ursu, Thin Solid Films 238, (1994) 276-279.
28. I.N. Mihailescu, A. Lita, V. S. Teodorescu, A. Luches, M. Martino, A. Perrone, M. Gartner, J. Mat. Sci. 31, (1996) 2839-2847.
29. R. Cireasa, A. Crunteanu, R. Alexandrescu, I. Morjan, C. Martin, I.N. Mihailescu, G. Oncioiu, Carbon 36, (1998) 775-780.
30. J. Neamtu, I.N. Mihailescu, C. Ristoscu, J. Hermann, J. Appl. Phys. 86(11), (1999) 6096-6106.
31. V. Nelea, C. Ristoscu, C. Chiritescu, C. Ghica, I. N. Mihailescu, A. Cornet, Appl. Surf. Sci. 168(1-4), (2000) 127-131.
32. 1. M. Cernea, I.N. Mihailescu, C. Martin, C. Ristoscu, M. Iliescu, J. Modern Opt. 48, (2001) 2185-2189.
33. C. Ristoscu, I.N. Mihailescu, M. Velegrakis, M. Massaouti, A. Klini, C. Fotakis, J. Appl. Phys. 93(5), (2003) 2244-2250.
34. G. Socol, P. Torricelli, B. Bracci, M. Iliescu, F. Miroiu, A. Bigi, J. Werckmann, I.N. Mihailescu, Biomaterials 25(13), (2004) 2539-2545.
35. R. Langer, D.A. Tirrel, Nature 428, 487-492, (2004).
36. A. Steinbuchel: *Biopolymers* (John Wiley-VCH, Weinheim 2003).
37. R.K. Singh, W.S. Kim, M. Ollinger, V. Craciun, I. Coowantwong, G. Hochhaus, N. Koshizaki, App. Surf. Sci. 197, (2002) 610-614.
38. J.D. Talton, J.M. Fitz-Gerald, R.K. Singh, G. Hochhaus, Respiratory Drug Delivery VII (2000), 67-74.
39. J.P. Vacanti, R. Langer, Lancet 354, 32-34 (1999).
40. J.C. Miller, R.F. Haglund, Jr., (Eds.), *Laser Ablation and Desorption,* Academic Press, 1998.
41. Y. Suginoshita, Y. Tabata, T. Matsumura, Y. Toda, M. Nabeshima, F. Moriyasu, Y. Ikada, T. Chiba, J. Controlled Release 83(1), (2002) 75-88.
42. Hayashibara, *Pullulan - A Big Breakthrough after 30 Years of Persistent Effort*, Development Story Nikkei Biotechnology & Business July, 2003.

43. M.V. Barnabas, J. Smets, F.A. Barnabas, M.S. Showell, *Treating Compositions Comprising Polysaccharides*, Patent No. 6,613,733 (2003).
44. M. Moscovici, C. Ionescu, C. Oniscu, O. Fotea, P. Protopopescu, L.D. Hanganu, Biotechnol. Let. 18(7), (1996) 787-790.
45. M. van der Rest, R. Garrone, FASEB J. 5(13), (1991) 2814-2823.
46. P. Budrugeac, V. Trandafir, M.G. Albu, J. Therm. Analys. Calorim. 72 (2), (2003) 581-585**.**
47. M. Hopkin, Nature January 12, 2004, http://www.nature.com/nsu/040105/040105-13.html.
48. M.J. Sever, J. T. Weisser, J. Monahan, S. Srinivasan, J.J. Wilker, Angewandte Chemie International Edition, 43 (4), (2004) 448-450.
49. A.J. Kinloch, MRS Bull., June 2003 445-448.
50. S. Gaidos, The Dallas Morning News, January 25, 2004.
51. T.J. Deming, Curr. Op. Chem. Biol. 3 (1), (1999) 100-105.
52. *Marine Models in Biomedical Research*, Biol. Bull. (176), (1989) 337-348.
53. J.H. Waite, *Reverse Engineering of Bioadhesion in Marine Mussels,* Ann N Y Acad Sci. 875, (1999) 301-309.
54. J.H. Waite, Integrative Comparative Biol. 42 (6), (2002) 1172-1180.
55. M.P. Olivieri, R.M. Wollman, M.I. Hurley, M.F. Swartz, Biofouling 18 (2), (2002)149-159.
56. J.L. Dalsin, B.-H. Hu, B.P. Lee, P.B. Messersmith, J. Am. Chem. Soc. 125 (14), (2003) 4253-4258.
57. C. Creton, E. Papon, (Guest Eds), MRS Bulletin, June 2003 419-423.
58. K. Michoud, Protein Spotlight 2, 2000.
59. L.O. Burzio, V.A. Burzio, T. Silva, L.A. Burzion, J. Pardo, Curr. Opin. Biotechnol. 8, (1997) 309-312.
60. P. Marks, The New Scientist Magazine, 164 (2209), (1999), 12.
61. C.T. Murray, R.L. Rudman, M.B. Sabade, A.V. Pocius, MRS Bulletin, June 2003, 449-454.
62. Committee on Marine Biotechnology: Biomedical Applications of Marine Natural Products, National Research Council, *Marine Biotechnology in the Twenty-First Century: Problems, Promise, and Products*, National Academy Press, 2002.
63. M. Yu, T.J. Deming, Macromolec. 31, (1998) 4739-4745.
64. M.E. Callow, J.A. Callow, Biologist (2002) 49 (1).
65. X. Qin, J.H. Waite, Journal of Experimental Biology 198, (1995) 633–644.
66. K. Huang, B.P. Lee, D.R. Ingram, P.B. Messersmith, Biomacromol. 3 (2), (2002) 8) 3145-3148.
67. J.C. Miller (Ed.), *Laser Ablation Principles and Applications*, Springer Verlag, Berlin, 1994.
68. M. Von Alleman, A. Blatter, *Laser-Beam Interactions with Materials: Physical Principles and Applications*, Springer-Verlag Berlin Heidelberg, 1995.
69. D.B. Chrisey, G.K. Hubler, (Eds.), *Pulsed Laser Deposition of Thin Films*, John Wiley & Sons, New York, 1994.
70. A. Pique, Chapter *Matrix Assisted Pulsed Laser Evaporation*, to appear in *Pulsed Laser Deposition of Thin Films: Applications in Electronics, Sensors, and Biomaterials*, edited by D.B. Chrisey and R.W. Eason, J. Wiley & Sons, Spring 2005.
71. R. D. Schaeffer, Laser Focus World 37 (6), June 2001, 217-219.
72. N. van Kampen, *Stochastic Processes in Physics and Chemistry*, North-Holland, Amsterdam, 1981.
73. H.M. Smith, A.F. Turner, Appl. Opt. 4 (1), (1965) 147-148.
74. I.N. Mihailescu, E. Gyorgy, *Pulsed Laser Deposition: An Overview,* in: *International Trends in Optics and Photonics,* T. Asakura (Ed.), Springer, Heidelberg, 1999.
75. D. Bauerle, *Laser Processing and Chemistry*, Springer-Verlag, 3rd edition, 2000.
76. D.M. Bubb, D.B. Chrisey, Lambda Physik Highlights, Summer 2004, No. 64.
77. D.B. Chrisey, A. Pique, R.A. McGill, J.S. Horwitz, B.R. Ringeisen, D.M. Bubb, P.K Wu, Chem. Rev. 103 (2), (2003) 553-576.
78. H. Niino, A. Yabe, Appl. Phys. Lett. 60 (21), (1992) 2697-2699.
79. R. Srinivasan, B. Braren, D.E. Seeger, R.W. Dreyfus, Macromolecules 19, (1986) 916-921.
80. **R. Cristescu**, G. Socol, I.N. Mihailescu, M. Popescu, F. Sava, E. Ion, C.O. Morosanu, I. Stamatin, **Appl. Surf. Sci.** 208-209, (2003) 645-650.
81. **R. Cristescu**, I. Stamatin, D.E. Mihaiescu, C. Ghica, M. Albulescu, I.N. Mihailescu, D.B. Chrisey, **Thin Solid Films** 453-454C, (2004) 262-268.
82. D.B. Chrisey, A. Pique, J.M. Fitz-Gerald, R.C.Y. Auyeng, R.A. McGill, H.D. Wu, M. Duignan, Appl. Surf. Sci. 154, (2000) 593-600.
83. J.M. Fitz-Gerald, G. Jennings, R. Johnson, C.L. Fraser, Appl. Phys. A (2003), December On line.
84. R.A. McGill, R. Chung, D.B. Chrisey, P.C. Dorsey, P. Mattews, A. Pique, T.E. Mlsna, J.I. Stepnowski, IEEE Trans. Ultrason. Ferroelectr. Freq. Control 45 (5), (1998) 1370-1380.
85. G.T. Tortora, B.R. Funke, C.L. Case, *Microbiology, an Introduction,* Benjamin/Cummings, Redwood City, CA, 1995.
86. V. Karbach, R. Knochenmuss, R. Zenobi, J. Am. Soc. *Mass Spectrum.* 9 (11), (1998) 1226-1228.
87. M.C. Fitzgerald, G.R. Parr, L.M. Smith, Anal. Chem. 65 (22), (1993) 3204-3211.

88. D.M. Bubb, P.K. Wu, J.S. Horwitz, J.H. Callahan, M. Galicia, A. Vertes, R.A. McGill, E.J. Houser, B.R. Ringeisen, D.B. Chrisey, J. Appl. Phys. 91 (4), (2002) 2055-2058.
89. M. Karas, D. Bachmann, U. Bahr, F. Hillenkamp, Int. J. Mass-Spectr. Ion Proc. 78, (1987) 53-68.
90. Vertes, in: K.G. Standing, W. Ens (Eds.), *Methods and Mechanisms for Producing Ions from Large Molecules*, Plenum Press, New York, 1998.
91. R. Kelly , A. Miotello, Nucl. Instrum. Methods Phys. Res. B 122, (1997) 374-400.
92. D.B. Geohegan, in *Pulsed Laser Deposition of Thin Films*, edited by D.B. Chrisey and G.K. Hubler ~Wiley, New York, 1994.
93. D. Bhattacharya, R.K. Singh, P.H. Holloway, J. Appl. Phys. 70, (1991) 5433-5439.
94. M.A Stevens, B.A. Weir, G.J. Denton, R.H. Friend, Synth. Met. 1999, 101, 234-235.
95. A. Pique, R.A. McGill, D.B. Chrisey, D. Leonhardt, T.E. Mslna, B.J. Spargo, J.H. Callahan, R.W. Vachet, R. Chung, M.A. Bucaro, Thin Solid Films 355-356, (1999) 536-541.
96. P.K. Wu, J. Fitz-Gerald, A. Piqué, D.B. Chrisey, R.A. McGill, MRS Proceedings 617 (2000) J2.3 1-6.
97. P.K. Wu, B.R. Ringeisen, J.H. Callahan, M. Brooks, D.M. Bubb, H.D. Wu, A. Pique, B.J. Spargo, R.A. McGill, D.B. Chrisey, Thin Solid Films 398, (2001) 607-614.
98. D.M. Bubb, B.R. Ringeisen, J.H. Callahan, M. Galicia, A. Vertes, J.S. Horwitz, R.A. McGill, E.J. Houser, P.K. Wu, A. Pique, D.B. Chrisey, Appl. Phys. A - Mater. Sci. & Process. 73(1), (2001) 121-123.
99. B.R. Ringeisen, J. Callahan, P.K. Wu, A. Pique, B.J. Spargo, R.A. McGill, M. Bucaro, H. Kim, D.M. Bubb, D.B. Chrisey, Langmuir 17(11), (2001) 3472-3479.
100. A. Pique, P. Wu, B.R. Ringensen, D.M. Bubb, J.S. Mellinger, R.A. McGill, D.B. Chrisey, Appl. Surf. Sci. 186(1-4), (2002) 408-415.
101. P.K. Wu, B.R. Ringeisen, D.B. Krizman, C.G. Frondoza, M. Brooks, D.M. Bubb, R.C.Y. Auyeung, A. Pique, B.J. Spargo, R.A. McGill, D.B. Chrisey, Rev. Sci. Instr. 74 (4), (2003) 2546-2557.
102. A. Pique, R.C.Y. Auyeung, J.L. Stepnowski, D.W. Weir, C.B. Arnold, R.A. McGill, D.B. Chrisey, Surf. Coat. Tech. 163, (2003) 293-299.
103. A. Gutiere-Llorente, R. Perez-Casero, B. Pajot, J. Russel, R.M. Defourneau, J.L. Fave, E. Millon, J. Perriere, Appl. Phys. A. 77, (2003) 785-788.
104. D.M. Bubb, S.M. O'Malley, C. Antonacci, D. Simonson, R.A. McGill, J. Appl. Phys. 95(4), (2004) 2175-2177.
105. B. Toftmann, M.R. Papantonakis, R.C.Y. Auyeung, W. Kim, S.M. O'Malley, D.M. Bubb, J.S. Horwitz, J. Schou, P.M. Johansen, R.F. Haglund, Jr, Thin Solid Films 453-454, (2004) 177-181.
106. V. Meenakshi, W. Teizer, D.G. Naugle, H. Zhao, K.R. Dunbar, Solid State Comm. 132 (2004) 471–476.
107. D.M. Bubb, M.R. Papantonakis, B. Toftmann, J.S. Horwitz, R.A. McGill, D.B. Chrisey, R.F. Haglund, J. Appl. Phys. 91 (12), (2002) 9809-9814.
108. L.I. Maissel, R. Glang, (Eds.), *Handbook of Thin Film Technology*, McGraw–Hill, New York, 1970.
109. L.V. Zhigilei, P.B.S. Kodali, B.J. Garrison. J. Phys. Chem. B 101, (1997) 2028-2037.
110. L.V. Zhigilei, P.B.S. Kodali, B.J. Garrison, J. Phys. Chem. B 102, (1998) 2845-2853.
111. L.V. Zhigilei, B.J. Garrison, Appl. Phys. Lett. 74 (9), (1999) 1341-1343.
112. L.V. Zhigilei, B.J. Garrison, Appl. Phys. A-Mat. Sci. & Process. 69, (1999) S75-S80.
113. L.V. Zhigilei, B.J. Garrison, J. Appl. Phys. 88 (3), (2000) 1281-1298.
114. L.V. Zhigilei, E. Leveugle, B.J. Garrison, Y.G. Yingling, M.I. Zeifman, Chem. Rev. 2003, 103, 321-347
115. T.E. Itina, L.V. Zhigilei, B.J. Garrison, Nucl. Instr. & Meth. Phys. Res. B 180, (2001) 238-244.
116. J. Neamtu, I.N. Mihailescu, C. Ristoscu, J. Hermann, J. Appl. Phys. 86(11), (1999) 6096-6106.
117. **R. Cristescu,** D. Mihaiescu, I. Stamatin, G. Socol, I.N. Mihailescu, D.B. Chrisey, **Appl. Phys. A - Mater. Sci. & Process**. 79 (4-6), (2004) 1023-1026.
118. **R. Cristescu**, T. Patz, R. Narayan, N. Menegazzo, B. Mizaikoff, D. Mihaiescu, P.B. Messersmith, I. Stamatin, I.N. Mihailescu, D.B. Chrisey, Accepted for publication in **Appl. Surf. Sci**., July 12, 2004.
119. F. Sava, **R. Cristescu**, G. Socol, R. Radvan, R. Savastru, D. Savastru, **J. Optoelectron. Adv. Mater**. 4 (4), (2002) 965-970.
120. E. F. Kaelble (Ed.) *Handbook of X-Rays*, McGraw-Hill Book Company, New York, 1967.
121. D. Briggs, M. P. Seah (Eds.), *Practical Surface Analysis by Auger and X-ray Photoelectron, Spectroscopy*, Wiley, Chichester, 1983.
122. M. Balaceanu, M. Braic, D. Macovei, M. J. Genet, A. Manea, D. Pantelica, V. Braic, F. Negoita, J Optoel. Adv. Mat. 4 (1), (2002) 107-114.
123. D. Sarangi, O.S. Panwar, S. Kumar, R. Battacharyya, J. Vac. Sci. Technol. A 18, (2000) 2302-2311.
124. G. Beamson, D. Briggs, (Eds.), *High Resolution XPS of Organic Polymers – The Scienta ESCA300 Database*, Wiley Interscience, 1992.
125. J.C. Lascovich, R. Giorgi, S. Scaglione, Appl. Surf. Sci. 47, (1991) 17-21.
126. **R. Cristescu**, G. Socol, I.N. Mihailescu, I. Morjan, I. Soare, M. Popescu, F. Sava, C.O. Morosanu, I. Stamatin, A. Andrei, J. Neamtu, **SPIE Proceedings** 5147, (2003) 87-94.

127. T. Yoshitake, T. Nishiyama, H. Aoki, K. Suizu, K. Takahashi, K. Nagayama, Appl. Surf. Sci. 141, (1999) 129-137.
128. P.R.Vinod, H. Kakiuki, T. Terai, A. N. Itakura, M. Kitajima, Int. J. Mod. Phys. B 16 (6-7), (2002) 1008-1012.
129. J.Y. Chen, L.P. Wang, K.Y. Fu, N. Huang, Y. Leng, P. Yang, J. Wang, G.J. Wan, H. Sun, X.B. Tian, P.K. Chu, Surf. & Coat. Techn. 156, (2002). 289-294.
130. H. Hiraoka, W.Y. Wong, T.M. Wong, SPIE Proceedings 3093 (27), (1997) 204-212.
131. M. Ouyang, H. Hiraoka, Mat. Sci. Engin. B 39, (1996) 228-231.
132. S. Latsch, H. Hiraoka, J. Min. Met. Mater. Soc. 46 (7), (1994) 64-65.
133. T. Shibata, K. Tonan, T. Yasuda, S.I. Ikawa, Appl. Spectrosc. 51 (3), (1997) 337-339.
134. **A. Vogel, V. Venugopalan, Chem. Rev. 103, (2003) 577-644.**
135.
136. D. Lin-Vien, N.B. Colthup, W.B. Fateley, J.B. Grasselli, *The Handbook of Infrared and Raman Characteristic Frequencies of Organic Molecules*, Academic Press, Inc. Boston, 1991.
137. KnowItAll Database by Bio-Rad Laboratories, http://www.bio-rad.com.
138. D. Cule, T. Hwa, Phys. Rev. Lett. 80 (14), (1998) 3145-3148.
139. T. Patz, **R. Cristescu**, R.J. Narayan, N. Menegazzo, B. Mizaikoff, P.B. Messersmith, J.J. Wilker, I. Stamatin, I.N. Mihailescu, D.B. Chrisey, Accepted for publication in **Appl. Surf. Sci.,** November, 2004.
140. L. Litauszki, L. Howard, L. Salvati, P.J. Tarcha, J. Biomed. Mater. Res. 35, (1997) 1-8.
141. V.N. Vasilets, C. Werner, G. Hermel, D. Pleul, M. Nitschke, A. Menning, A. Janke, F. Simon, J. Adhesion Sci. Technol. 16, (2002) 1855-1868.
142. A.M. Baty, P.K. Leavitt, C.A. Siedlecki, B.J. Tyler, P.A. Suci, R.E. Marchant, G.G. Geesey, Langmuir 13, (1997) 5702-5710.
143. M Olivieri, R. Baier, R Loomis, Biomaterials 13, (1992) 1000-1008.
144. M. Zilberman, R.C. Eberhart, N.D. Schwade, J. Biomater. Sci. Polymer Edn. 13, (2002) 1221-1240.
145. H. Rangwalla, A.D. Schwab, B. Yurdumakan, D.G. Yablon, M. S. Yeganeh, A. Dhinojwala, Langmuir 20 (20), (2004) 8625-8633.